Phase diagrams of electric-field-induced aggregation in conducting colloidal suspensions

Boris Khusid*
Department of Mechanical Engineering, New Jersey Institute of Technology, University Heights, Newark, New Jersey 07102

Andreas Acrivos†
The Levich Institute, City College of the City University of New York, Steinman Hall, 140th Street & Convent Avenue, New York, New York 10031

(Received 24 February 1999)

To develop a theory for electric-field-driven phase transitions in *concentrated* suspensions, we extended our microscopic theory [Phys. Rev. E **52**, 1669, (1995); **54**, 5428, (1996)] beyond the *dilute* regime. Based on the model of the Maxwell-Wagner interfacial polarization of colloids, our theory overcomes the limitations of Brillouin's formula for the electric energy of conducting materials which is applicable only for negligibly small energy dissipation and slow time variations of the field. We found that the phase diagrams of ''the particle concentration vs the electric field strength'' for colloids are similar to the phase diagrams for the first-order phase separation in quenched conventional binary systems with a high-temperature miscibility gap. This explains why a variety of colloids exhibit similar field-induced aggregation patterns. Our theory provides a reasonable interpretation of the available experimental data on field-induced aggregation phenomena in electrorheological fluids and aqueous suspensions, whereas currently used theoretical models are in variance with many of the data. The theoretical results enable one to trace how the variations of the electrical properties of the constituent materials influence the topology of the suspension phase diagram and to evaluate the effects of the field strength and frequency on the particle aggregation. [S1063-651X(99)14208-9]

PACS number(s): 82.70.Dd, 47.55.Kf, 47.65.+a, 64.75.+g

I. INTRODUCTION

Under the application of a sufficiently strong electric field, a conducting colloidal suspension may undergo reversible phase transitions from a homogeneous random arrangement of particles into a variety of ordered aggregation patterns. The evolution of these structures can easily be manipulated by varying the frequency and strength of the applied field, both of which strongly influence the interactions among colloidal particles responsible for such effects. But in spite of numerous applications in biotechnology, separations, electrorheology, the processing of materials, microdevices for chemical analysis, etc., which have expanded rapidly over the last decade, our understanding of how the electrical properties of the constituent materials influence the electric-field-driven aggregation in conducting suspensions is far from complete.

The surprising fact about such electric-field-induced phase transitions is that the aggregation patterns, which are observed in very diverse systems of colloidal suspensions, display a number of common structural features and modes of evolution, thereby implying that a universal mechanism may exist to account for these electric-field-driven phenomena. It is now generally believed that this mechanism emanates from the presence of the long-range anisotropic interactions between colloidal particles due to their polarization in an applied field.

The first step in the development of a theory for the electric-field-induced phase transitions in a suspension of electrically uncharged conducting particles dispersed in a conducting fluid was taken in Refs. [1,2]. To begin with, the free energy of a conducting suspension containing N randomly arranged hard spheres subject to an electric field was written (Ref. [1], Sec. II) as

$$F=\left[\frac{k_BT}{v_p}f_0(c)-W\right]V, \tag{1}$$

where the first term in Eq. (1) refers to the free energy of a suspension, in the absence of the electric field, as a function of the volume V, the temperature T with k_B being Boltzmann's constant, and the volume concentration of the particles, $c=v_pN/V$, with v_p being the particle volume; the second term in Eq. (1) refers to the electric energy of a suspension caused by the interaction of the particles with the applied electric field and by the electric-field-induced long-range interparticle interactions.

The concentration dependence of the function $f_0(c)$ in Eq. (1) is well understood [3,4]. Specifically, it can be related to the suspension compressibility factor $Z(c)$ [with $Z(c)\to 1$ for $c\to 0$] by means of

$$f_0(c)=c\ln\frac{c}{e}+c\int_0^c\frac{Z(c)-1}{c}dc,$$

where, for a suspension in the disordered state, $Z(c)$ is given approximately by, for example [3,4], the Carnahan-Starling equation

$$Z(c)=\frac{1+c+c^2-c^3}{(1-c)^3}\quad\text{when}\quad 0<c\leqslant 0.5 \tag{2a}$$

*Electronic address: khusid@admin.njit.edu
†Electronic address: acrivos@scisun.sci.ccny.cuny.edu

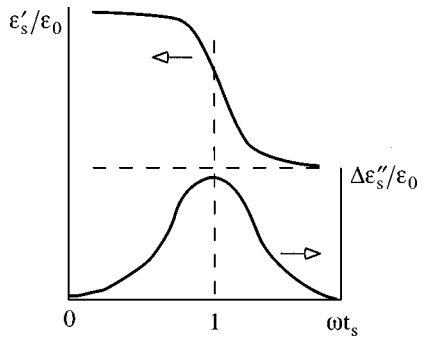

FIG. 1. Frequency variation of the real component (ε_s') and the excess of the imaginary component over the static conductivity ($\Delta\varepsilon_s''=\varepsilon_s''-\sigma_s|_{\omega=0}/\omega$) of the complex dielectric permittivity $\varepsilon_s^*=\varepsilon_s'-i\varepsilon_s''$ for a dielectric with a single relaxation process; ε_0 is the vacuum permittivity.

and by

$$Z(c)\approx\frac{A}{c_m-c} \quad \text{with } A\sim 1.85 \quad \text{as } c\to c_m, \qquad (2b)$$

where $c_m\sim 0.63-0.64$ corresponds the concentration of the spheres at random close packing. Recall that, in the absence of an electric field, a suspension of hard spheres is stable approximately for $c\leqslant 0.50-0.55$ whereas for $0.55<c<0.74$ it may undergo a transition from a disordered state to an ordered face-centered-cubic structure [3,4].

The main obstacle which had to be overcome in constructing a theory of electric-field-induced phase transitions was that, for materials such as conducting suspensions whose complex dielectric permittivity $\varepsilon_s^*=\varepsilon_s'-i\varepsilon_s''$ varies strongly with the frequency of the applied electric field, the electric energy density W in Eq. (1) cannot be constructed using macroscopic electrodynamics [5]. For example, Fig. 1 illustrates a common feature of the frequency variation of the real component ε_s' and imaginary component ε_s'' for conducting suspensions, specifically, the presence of one, as shown in Fig. 1, or more dielectric relaxation processes with characteristic relaxation times. Recall that ε_s' gives the dielectric constant of a material, whereas ε_s'' determines the power dissipation (loss factor) in this material due to its conductivity. The reason for the difficulty in constructing the electric energy for a conducting material is that such a material contains mobile charges which dissipate electric energy and electric dipoles which store electric energy, which implies that the total electric energy stored by a conducting material will depend on the time history of how the electric field was established [6].

To be sure, an expression for the electric energy density W of a conducting material, namely, Brillouin's formula [see Eq. (3) below], can be derived from macroscopic electrodynamics [5,6], but only when the energy dissipation in this material is negligibly small and the time variations of the applied electric field are very slow as compared to the rate of the relaxation phenomena, i.e.,

$$W=\frac{1}{2}\frac{d}{d\omega}[\omega\varepsilon_s'(\omega)]\langle E^2(\omega)\rangle_T \qquad (3)$$

only if

$$|\varepsilon_s''(\omega)|\ll\varepsilon_s'(\omega) \quad \text{and} \quad \omega t_s\ll 1,$$

where ω and $E(\omega)$ are the frequency and Fourier amplitude of the applied electric field, respectively, t_s is the relaxation time of the dielectric phenomena, and $\langle\ldots\rangle_T$ denotes the time average. As can be seen from Eq. (3), Brillouin's formula is applicable only under the severe limitations that conductivity effects be negligibly small so as not to cause losses in the stored electric energy. That is why Brillouin's formula can be utilized in Eq. (1) to describe electric-field-driven phase transformations in conducting colloids only, as can be seen in Fig. 1, at very low frequencies far to the left of the relaxation peak.

To overcome the limitations of Brillouin's formula, we developed [1] a microscopic theory for the electric energy density W of conducting spheres dispersed in a conducting fluid when the particles were arranged randomly and provided that the particles and suspending fluid can be described by the model of a leaky dielectric, i.e., when their dielectric constants ε_p and ε_f and conductivities σ_p and σ_f are frequency independent. This model corresponds to the classical mechanism of the Maxwell-Wagner interfacial polarization typical of colloids [7–9]. In this case, the short-term polarization of the particles and fluid is determined solely by their instantaneous polarization, whereas their long-term polarization arises from the buildup of charge at the interface between the particles and surrounding fluid. We exploited two microstructure-based techniques for calculating the electric energy density. One of them is based on a mean-field approximation (a cell model) where the average field acting on each particle is considered to be the well-known Lorentz-Lorenz local field [5,6] rather than the applied field, while the second made use of statistical methods for determining the average properties of dilute suspensions. To calculate, on the basis of the second method, the first two terms in the expansion for the electric energy density W as a power series in the particle concentration c, we also had to use a renormalization technique in order to overcome the difficulty associated with the fact that the integral of the energy of the long-range dipole-dipole interaction between two particles is only conditionally convergent. But as we found [1], the main contribution to the electric energy of a suspension, as well as to its complex permittivity, is given by those multiparticle interactions which lead to a change in the local electric field acting on a particle. That is the reason why, for example, the cell model, which accounts only for this effect, yields the well-known Maxwell-Wagner expression for the complex permittivity of a suspension which correlates well with experimental data [7].

The theory of Ref. [1] relates the electric energy density of a conducting suspension to the dielectric constants and conductivities of the particles and suspending fluid, particle concentration, and frequency and strength of the applied electric field. To illustrate the advantages of this theory, the first two terms in the expansion of the electric energy density W in powers of the particle concentration were substituted in Eq. (1), which was then used to study the phase separation of a dilute conducting suspension subject to strong electric fields [1]. On this basis, we then calculated in Refs. [1,2] the critical conditions beyond which the random arrangement of the particles becomes unstable in the presence of spatially

uniform and nonuniform electric fields.

The main objective of the present work is to extend our previous studies [1,2] beyond the dilute regime and to develop a microscopic theory for phase diagrams of *concentrated* conducting suspensions subject to strong dc and ac electric fields. To this end, we employ in Eq. (1) the full expression for the free energy density W of a conducting suspension, as a function of a concentration, which we derived in Ref. [1], Sec. IV A, using the mean-field approximation, and then investigate the topology of the suspension phase diagram, i.e., ''the particle concentration vs the electric field strength,'' and relate it to the electrical properties of the constituent materials.

A peculiarity of concentrated suspensions is that the sign of the electric energy density of the interparticle interactions, i.e., $\partial^2 W/\partial c^2$, may change at some value of the concentration. As a result of this feature, which is absent in the theory for dilute systems [1], several types (in fact, six) of phase diagrams of conducting suspensions can occur because the ability or inability of the particles to aggregate in the presence of applied electric fields depends on the particle concentration as well. The results to be obtained, which include those in Refs. [1,2] as limiting cases, yield the phase diagrams of a suspension as a function of the mismatch of the dielectric constants, of the conductivities of the particles, and of the fluid and frequency of the applied field. This, as we shall see, provides a framework for interpreting a variety of experimental data which appear, at first glance, to be unrelated. In addition, we will demonstrate that similarities exist between particle aggregation under the action of electric fields and phase transformations in quenched atomic systems. Although such a similarity between the structural ordering in colloids and the structural behavior in conventional atomic systems—gas, liquid, crystal, and glasses—under suitable conditions has already been well recorded [3,4], electric-field-driven phase transitions in colloids have not been treated from this point of view thus far.

We begin in Sec. II by discussing the similarity between the action of electric fields on colloids and the quenching of atomic systems. Next, in Sec. III we proceed to develop a classification scheme of the topologies of the phase diagrams of concentrated suspensions subject to dc electric fields, while in Sec. IV we demonstrate that this classification scheme includes phase diagrams for suspensions subject to ac electric fields as well. Unfortunately, a description of the disorder-to-order transformations in a high-concentration phase cannot be included in these diagrams because of the absence of an equation for the free energy of anisotropic conducting aggregates, which is required. In Sec. V we shall consider how a spatial nonuniformity of an electric field can contribute to aggregation phenomena, while Sec. VI contains a comparison between the relevant theoretical predictions and currently available experimental data. Specifically, we will demonstrate how these data can be interpreted within the context of our theory and then discuss why the currently used theoretical models are unable to provide a unifying framework for explaining this body of experimental results. Section VII summarizes the main results from our studies. These enable one to trace how the variations of the electrical properties of the constituent materials influence the topology of the suspension phase diagram and then, by using an appropriate phase diagram, to evaluate how the electric-field-induced transformations will depend on the strength of the applied field and particle concentration.

II. ELECTRIC-FIELD-INDUCED PHASE TRANSITIONS

As was shown in Ref. [1], the expression for the electric energy density W of a conducting suspension being subjected to a dc electric field E for short and for long times becomes, respectively,

$$W=\frac{\varepsilon_f}{2}\frac{1+2c\dfrac{\varepsilon_p-\varepsilon_f}{\varepsilon_p+2\varepsilon_f}}{1-c\dfrac{\varepsilon_p-\varepsilon_f}{\varepsilon_p+2\varepsilon_f}}E^2 \quad \text{as} \quad t\ll t_s, \tag{4a}$$

$$W=\left[\frac{\varepsilon_f}{2}\frac{1+2c\dfrac{\varepsilon_p-\varepsilon_f}{\varepsilon_p+2\varepsilon_f}}{1-c\dfrac{\varepsilon_p-\varepsilon_f}{\varepsilon_p+2\varepsilon_f}}+\frac{9c(1-c)(\varepsilon_f\sigma_p-\varepsilon_p\sigma_f)^2}{2(\varepsilon_p+2\varepsilon_f)\left(1-c\dfrac{\varepsilon_p-\varepsilon_f}{\varepsilon_p+2\varepsilon_f}\right)(\sigma_p+2\sigma_f)^2\left(1-c\dfrac{\sigma_p-\sigma_f}{\sigma_p+2\sigma_f}\right)^2}\right]E^2, \tag{4b}$$

as $t\gg t_s$, while for an ac electric field $E_0\cos\omega t$ and for the long-term $t\gg t_s$ regime the equation for the time average of the electric energy of a suspension is [1]

$$W=\frac{\varepsilon_f}{4}\frac{1+2c\dfrac{\varepsilon_p-\varepsilon_f}{\varepsilon_p+2\varepsilon_f}}{1-c\dfrac{\varepsilon_p-\varepsilon_f}{\varepsilon_p+2\varepsilon_f}}E_0^2+\frac{9c(1-c)(\varepsilon_f\sigma_p-\varepsilon_p\sigma_f)^2E_0^2}{4(1+\omega^2t_s^2)(\varepsilon_p+2\varepsilon_f)\left(1-c\dfrac{\varepsilon_p-\varepsilon_f}{\varepsilon_p+2\varepsilon_f}\right)(\sigma_p+2\sigma_f)^2\left(1-c\dfrac{\sigma_p-\sigma_f}{\sigma_p+2\sigma_f}\right)^2} \tag{5}$$

$$\text{with} \quad t_s = \frac{(\varepsilon_p + 2\varepsilon_f)\left(1 - c\,\dfrac{\varepsilon_p - \varepsilon_f}{\varepsilon_p + 2\varepsilon_f}\right)}{(\sigma_p + 2\sigma_f)\left(1 - c\,\dfrac{\sigma_p - \sigma_f}{\sigma_p + 2\sigma_f}\right)}.$$

For brevity, we included the vacuum permittivity ε_0 as a multiplier in the definition of the dielectric constants ε_p and ε_f in Eqs. (4) and (5).

Equation (4a) and the first terms in Eqs. (4b) and (5), which are determined solely by the instantaneous polarization of the particles and fluid, are consistent with the relationship for the electric energy of a nonconducting suspension given by macroscopic electrodynamics [5],

$$W = \frac{1}{2}\varepsilon_s(c)E^2, \tag{6a}$$

with $\varepsilon_s(c)$ given by Maxwell's equation [7–9]

$$\varepsilon_s(c) = \varepsilon_f \frac{1 + 2\beta c}{1 - \beta c} \quad \text{with} \quad \beta = \frac{\varepsilon_p - \varepsilon_f}{\varepsilon_p + 2\varepsilon_f}. \tag{6b}$$

The second terms in Eqs. (4b) and (5) correspond to the energy required to build the charge at the particle surface and to redistribute the electric field inside the particles and suspending fluid when the time constants of the particles and fluid are different; that is when $\varepsilon_f/\sigma_f \neq \varepsilon_p/\sigma_p$ (see [1] for more details). But since the second term in Eq. (5) approaches zero as $\omega t_s \to \infty$, the electric energy of the suspension for high frequencies becomes the same as that for a nonconducting material, Eqs. (6a) and (6b). On the other hand, for a slowly varying electric field, $\omega t_s \ll 1$, Eq. (5) yields the expression for the time average of the electric energy which is consistent with the expression given by substituting the Maxwell-Wagner relation for $\varepsilon_s'(\omega)$ into Brillouin's formula, Eq. (3) (see [1] for more details).

Now, the osmotic pressure of a suspension Π [equal to $-(\partial F/\partial V)_{N,T,E}$ [10]] and the chemical potential of a particle μ [equal to $(F + \Pi V)/N$ [10]] can be evaluated from the equation of the free energy, Eq. (1), and are given by

$$\frac{\Pi v_p}{k_B T} = cZ(c) + \frac{v_p}{k_B T}\left(W - c\,\frac{\partial W}{\partial c}\right), \tag{7a}$$

$$\frac{\mu}{k_B T} = f_0'(c) - \frac{\partial}{\partial c}\left(\frac{W v_p}{k_B T}\right) \quad \text{with}$$

$$f_0' = \ln c + Z(c) - 1 + \int_0^c \frac{Z(c) - 1}{c}\,dc \tag{7b}$$

where the first terms in Eqs. (7) represent the osmotic pressure and chemical potential in the absence of an electric field, whereas the second terms account for the effect of the electric-field-induced long-range interparticle interactions. Notice that, in the absence of interparticle interactions, $W - c\,\partial W/\partial c$ and $\partial W/\partial c$ would become independent of the particle concentration since an increase in the suspension energy would be linearly proportional to the number of particles.

The random arrangement of the particles in a suspension is stable as long as the osmotic pressure increases with concentration, i.e.,

$$\frac{\partial}{\partial c}\left(\frac{\Pi v_p}{k_B T}\right) = Z + c\,\frac{dZ}{dc} - c\,\frac{\partial^2}{\partial c^2}\left(\frac{W v_p}{k_B T}\right) > 0. \tag{8}$$

Consequently, as seen from Eq. (8), as long as the third term on the right-hand-side is positive, in other words, as long as the interparticle interactions increase the suspension energy, an increase in the strength of the electric field [see Eqs. (4) and (5)] decreases the value of $\partial\Pi/\partial c$ and finally renders the random arrangement of the particles unstable when

$$\frac{\partial \Pi}{\partial c} = 0. \tag{9}$$

Now, Eq. (9) represents the spinodal curve in an equilibrium phase diagram of particle concentration vs the electric field strength of a conducting suspension subject to an electric field. Specifically, this curve is the locus of points for which the curvature of the suspension free energy changes from convex to concave [10].

For the case when $\partial^2 W/\partial c^2 > 0$ over the entire range $0 \leqslant c < c_m$, the spinodal points exist over the entire concentration range as well, so that increasing the strength of an electric field applied to this suspension will eventually cause an electric-field-induced transition. Thus the phase diagram of such a suspension consists of the low-field one-phase region, which includes the random spatial arrangement of the particles in the absence of an electric field, and the high-field two-phase region corresponding to the appearance of aggregates caused by the action of an applied field. This phase diagram appears to be similar to the concentration vs temperature phase diagram of a binary fluid or a binary alloy with a miscibility gap [10], so that these species exist in solution at high temperature, but their mixture eventually separates into coexisting phases below the critical point of miscibility. In this regard, the application of an electric field to a conducting suspension is equivalent to a quench of an atomic system from its high-temperature one-phase state.

The critical point on the spinodal curve of the suspension coincides with the inflection point of Π as a function of c, so that Eq. (9) has a multiple root. The parameters of the critical point, namely, c_{cr} and E^2_{cr}, are determined from the condition

$$\frac{\partial \Pi}{\partial c} = \frac{\partial^2 \Pi}{\partial c^2} = 0. \tag{10}$$

In a two-phase region (at $E^2 \geqslant E^2_{\mathrm{cr}}$), the values of the osmotic pressure and chemical potential of the particles in the coex-

isting phases are equal. The latter leads to the following relations [10] between the particle concentrations in the both phases, c_1 and c_2, respectively:

$$\mu(c_1)=\mu(c_2) \quad \text{and}$$

$$\Pi(c_1)=\Pi(c_2) \quad \text{or its equivalent} \quad \int_{c_1}^{c_2}\mu(c)dc=0. \tag{11}$$

Now, Eqs. (11) represent the coexistence curve in the phase diagram of a suspension. This curve is located to the left of the spinodal curve in the low-concentration part of the phase diagram and to the right of the spinodal curve in the high-concentration part of this diagram. Moreover, $c_1 \rightarrow c_{\rm cr}$ and $c_2 \rightarrow c_{\rm cr}$ as $E \rightarrow E_{\rm cr}$.

On the other hand, if the third term on the right-hand-side of Eq. (8) is negative, in other words, when the long-range interparticle interactions lower the suspension energy (i.e., when $\partial^2 W/\partial c^2 < 0$ over the entire range $0 \leqslant c < c_m$), an increase in the strength of the applied electric field increases the value of $\partial\Pi/\partial c$. In this case, the random spatial arrangement of the particles appears to be stable, so that the phase diagram of such a suspension reduces to the one-phase domain.

As can be seen from Eqs. (4) and (5), the sign of $\partial^2 W/\partial c^2$ depends on the particle-to-fluid ratios of the conductivities and dielectric constants, the frequency of the applied electric field, and the particle concentration. For a high-frequency electric field when $\omega t_s \rightarrow \infty$, Eq. (5) yields [see Eq. (6b) for β]

$$W=\frac{\varepsilon_f}{4}\frac{1+2c\beta}{1-c\beta}E_0^2, \tag{12a}$$

so that, at $\beta \neq 0$,

$$\frac{\partial^2 W}{\partial c^2}=\frac{3\varepsilon_f \beta^2 E_0^2}{2(1-\beta c)^3}>0 \quad \text{over} \quad 0 \leqslant c < c_m. \tag{12b}$$

Thus the sign of $\partial^2 W/\partial c^2$ always becomes positive when the frequency of the applied electric field becomes sufficiently high. Hence it follows that there always exists a threshold value of the frequency, above which the particles having a dielectric constant different from that of the suspending fluid (regardless of the mismatch of their conductivities, σ_p/σ_f) will aggregate as the strength of an applied electric field becomes sufficiently large. However, as we shall see, the sign of $\partial^2 W/\partial c^2$ may become negative for low frequencies. If this happens over the entire concentration range $0 \leqslant c < c_m$, the electric-field-induced aggregation of the particles will not occur at all. A peculiar feature of a concentrated suspensions is that, as we mentioned in Sec. I, the sign of $\partial^2 W/\partial c^2$ may change at some value of the concentration.

As in the case of conventional atomic systems [10], the use of a phase diagram provides a convenient way to distinguish ''metastable'' and ''unstable'' states of a suspension subject to an electric field, where we refer to the domain between the coexistence and spinodal curves in its phase diagram as metastable, and the domain beyond the spinodal line as unstable. The free energy of a suspension, being considered as a function of the particle concentration, is convex in the metastable region of the phase diagram of ''the particle concentration vs the electric field strength,'' so that the free energy will increase with a spontaneous concentration fluctuation, giving rise to an energetic barrier that will stabilize the suspension. The free energy, however, turns into a concave function of the particle concentration in the unstable region of the phase diagram, so that no energetic barrier to phase separation will exist in this state. This distinction can correspond to two different mechanisms of electric-field-induced transformations in a suspension: spinodal decomposition and nucleation, as occurs in atomic systems. For atomic systems, the former (in the unstable domain) corresponds to the growth of long-wavelength spontaneous concentration fluctuations with time, whereas the nucleation of microdomains of the other phase starts the transformation for the latter (in the metastable domain) [10,11]. However, as recent research demonstrates [11], there is no sharp dividing line between nucleation and spinodal transformations in atomic systems. Rather there exists a gradual transition in the dynamical behavior of a quenched system as the quench point on its phase diagram varies from one domain to the other in the vicinity of the spinodal curve.

In any event, we can expect that there exists some similarity between how spinodal and nucleation transformations operate in a suspension subject to an electric field and how they operate in quenched atomic systems, even though the electric-field-induced interparticle interactions are anisotropic. In this connection, we proceed in Secs. III and IV to construct, based on Eqs. (9) and (11), a classification scheme which can predict how the topology of the suspension phase diagram of ''the particle concentration vs the electric field strength'' depends on the particle and fluid dielectric constants and conductivities and the frequency of applied field. This will make it possible to exploit the great body of experimental data and theoretical predictions available for the quenching of atomic systems and use it as a framework for interpreting the morphology and kinetics of aggregation patterns in colloidal suspensions generated by the application of electric fields.

III. PHASE DIAGRAMS OF SUSPENSIONS SUBJECT TO dc FIELDS

A. Asymptotic behavior of the spinodal and coexistence curves

When a suspension is subjected to a dc electric field E over a long period of time ($t \gg t_s$), the substitution of Eqs. (4b) for its electric energy into Eqs. (9) and (11) yields the following expressions: for the spinodal curve,

$$Z+c\frac{dZ}{dc}-\lambda c\Psi_0=0, \tag{13}$$

and for the coexistence curve, with c_1 and c_2 corresponding to its low- and high-concentration parts, respectively,

$$f_0'(c_2)-f_0'(c_1)-\lambda\int_{c_1}^{c_2}\Psi_0 dc=0, \tag{14a}$$

$$c_2 Z(c_2)-c_1 Z(c_1)-\lambda\int_{c_1}^{c_2} c\Psi_0 dc=0, \tag{14b}$$

where

$$\Psi_0 \equiv \frac{\partial^2}{\partial c^2}\left(\frac{W}{\varepsilon_f E^2}\right)\Bigg|_{\omega=0} = \frac{3\left(\frac{\sigma_p}{\sigma_f}-1\right)\left[4-c+(2+c)\frac{\sigma_p}{\sigma_f}\right]}{\left[2+c+(1-c)\frac{\sigma_p}{\sigma_f}\right]^4}\left\{3\frac{\varepsilon_p}{\varepsilon_f}-\frac{2(2+c)+6(2-c)\frac{\sigma_p}{\sigma_f}+3(1+c)\left(\frac{\sigma_p}{\sigma_f}\right)^2-(1-c)\left(\frac{\sigma_p}{\sigma_f}\right)^3}{\left[4-c+(2+c)\frac{\sigma_p}{\sigma_f}\right]}\right\} \tag{15}$$

is the nondimensional function which represents the energy of the long-range interparticle interactions under dc fields, and the positive parameter $\lambda=\varepsilon_f E^2 v_p/k_B T$, being the ratio of the electric energy and thermal energy, is, on the one hand, a measure of the relative strength of the applied dc field. The last terms in Eqs. (14) follow from the relations

$$\left.\frac{\partial W}{\partial c}\right|_{c_2} - \left.\frac{\partial W}{\partial c}\right|_{c_1} = \int_{c_1}^{c_2}\frac{\partial^2 W}{\partial c^2}dc$$

and $$\left.\left(W-c\frac{\partial W}{\partial c}\right)\right|_{c_2} - \left.\left(W-c\frac{\partial W}{\partial c}\right)\right|_{c_1} = -\int_{c_1}^{c_2} c\frac{\partial^2 W}{\partial c^2}dc.$$

We can view Eq. (13) as giving us a function $\lambda(c)$ along the spinodal curve on the phase diagram of a suspension. Then Eqs. (10) for the critical points λ_{cr} and c_{cr} correspond to a minimum of this function. As follows from Eq. (13), Ψ_0 should be positive at least over some concentration range if the spinodal curve is to appear on the phase diagram.

As can be seen from Eq. (15), the equation $\Psi_0(\varepsilon_p/\varepsilon_f,\sigma_p/\sigma_f,c)=0$ in the σ_p/σ_f and $\varepsilon_p/\varepsilon_f$ plane has two roots. One of them is $\sigma_p=\sigma_f$, whereas the other gives $\varepsilon_p/\varepsilon_f$ as a function of σ_p/σ_f and c. As an illustration, we show in Fig. 2 a family of curves $\Psi_0(\varepsilon_p/\varepsilon_f,\sigma_p/\sigma_f,c)=0$ in the plane of σ_p/σ_f and $\varepsilon_p/\varepsilon_f$ for several values of the particle concentration. Clearly, as seen in this figure, Ψ_0 is positive only within two domains, one of which is located in the region of $\sigma_p>\sigma_f$ above the curve $\Psi_0=0$, whereas the other is in the region of $\sigma_p<\sigma_f$ below the curve $\Psi_0=0$. Also, along the curves $\Psi_0=0$, the sign of the variation of $\varepsilon_p/\varepsilon_f$ with concentration along the lines $\sigma_p/\sigma_f=\text{const}\neq 1$, namely,

$$\left(\frac{\delta\varepsilon_p/\varepsilon_f}{\delta c}\right)_{\sigma_p/\sigma_f,\Psi_0=0} = \frac{[4-c+(2+c)\sigma_p/\sigma_f]^2}{(\sigma_p/\sigma_f-1)^2(\sigma_p/\sigma_f+2)^2},$$

is always positive. Hence, as can also be seen from Fig. 2, a necessary condition for a conducting suspension to undergo a phase transition in dc fields is that the particle-to-fluid ratios of the dielectric constants and conductivities should lead to positive values of $\Psi_0(\varepsilon_p/\varepsilon_f,\sigma_p/\sigma_f,0)$ when the particle conductivity is larger than that of the fluid or to positive values of $\Psi_0(\varepsilon_p/\varepsilon_f,\sigma_p/\sigma_f,c_m)$ when the fluid conductivity is larger than that of the particles. This means that the random arrangement of these particles should become unstable, at least in the case of a dilute suspension as $c\to 0$ for the former case or as $c\to c_m$ for the latter. If, however, Ψ_0 changes sign at some concentration, say, c_r, so that $\Psi_0(\varepsilon_p/\varepsilon_f,\sigma_p/\sigma_f,c_r)=0$, then the spinodal curve will appear on the suspension phase diagram in the range $0<c<c_r$ for $\sigma_p>\sigma_f$ and in the range $c_r<c<c_m$ for $\sigma_p<\sigma_f$, respectively.

Let us consider the asymptotic behavior of the spinodal curve in the presence of strong fields, i.e., when $\lambda\to\infty$. On using Eq. (13) and the asymptotic expressions for $Z(c)$ as $c\to 0$ and $c\to c_m$ [see Eqs. (2a) and (2b), respectively], specifically, that $Z\to 1$ and $Z'=O(1)$ as $c\to 0$, whereas $Z,Z'\to\infty$ and $Z/Z'\to 0$ as $c\to c_m$, we arrive at the following expressions:

$$\lambda\approx 1/c\Psi_0(\varepsilon_p/\varepsilon_f,\sigma_p/\sigma_f,0) \quad \text{as } c\to 0, \tag{16a}$$

$$\lambda\approx Z'(c)/\Psi_0(\varepsilon_p/\varepsilon_f,\sigma_p/\sigma_f,c_m) \quad \text{as } c\to c_m, \tag{16b}$$

$$\lambda\approx (Z+cZ')_{c_r}/c_r\Psi_0(\varepsilon_p/\varepsilon_f,\sigma_p/\sigma_f,c) \quad \text{as } c\to c_r$$

$$\text{where } \Psi_0\approx\left.\frac{\partial\Psi_0}{\partial c}\right|_{c_r}(c-c_r). \tag{16c}$$

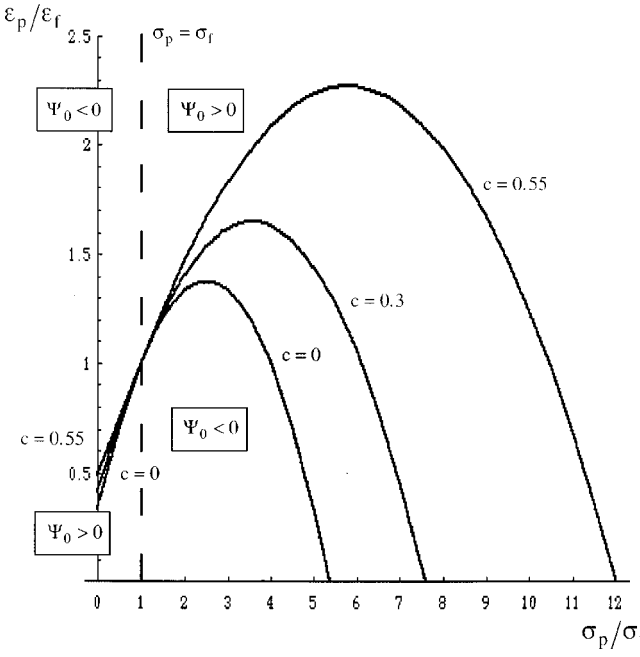

FIG. 2. Family of curves $\Psi_0(\varepsilon_p/\varepsilon_f,\sigma_p/\sigma_f,c)=0$ in the σ_p/σ_f and $\varepsilon_p/\varepsilon_f$ plane for $c=0$, 0.3, and 0.55; $\Psi_0(\varepsilon_p/\varepsilon_f,\sigma_p/\sigma_f,c)$ is positive above the corresponding curve in the region of $\sigma_p>\sigma_f$ and below it in the region of $\sigma_p<\sigma_f$.

Now consider the asymptotic behavior of the coexistence curve, Eqs. (14), as $\lambda \to \infty$. In the event that $\sigma_p > \sigma_f$, the smaller root of Eqs. (14), c_1, approaches zero as $\lambda \to \infty$. Hence, as follows from Eq. (16b), the limiting value of c_2, the larger root of Eqs. (16), depends on how the integral $\int_0^c c\Psi_0 dc$ decreases with increasing concentration c when $c > c_r$ where Ψ_0 becomes negative. As long as this integral equals zero at some concentration, say, c_2^a which is smaller than c_m, we obtain

$$c_2 \approx c_2^a + \frac{Z(c_2^a)}{\lambda \Psi_0|_{c_2^a}} \quad \text{and} \quad \ln c_1 \approx f_0'(c_2^a) - \lambda \int_0^{c_2^a} \Psi_0 dc \qquad (17a)$$

$$\text{at } \lambda \to \infty,$$

with $\int_0^{c_2^a} c\Psi_0 dc = 0$ and $\Psi_0|_{c_2^a} < 0$. On the other hand, if $\int_0^{c_m} c\Psi_0 dc > 0$, c_2 approaches c_m. In that case, on using the asymptotic relation $f_0'(c_2) - Z(c_2) = (A/c_m)\ln(c_m - c_2) + O(1)$ as $c \to c_m$ [see Eqs. (2b) and (7b)], we arrive at the following expressions:

$$\lambda \approx \frac{c_m Z(c_2)}{\int_0^{c_m} c\Psi_0 dc} \quad \text{and}$$

$$\ln c_1 \approx -\frac{\lambda}{c_m} \int_0^{c_m} (c_m - c)\Psi_0 dc + f_0'(c_2) - Z(c_2) \qquad (17b)$$

$$\text{at } c_2 \to c_m.$$

The right-hand side of the first expression in Eqs. (17b) is required to be positive in order for $\lambda \to \infty$ as $c_2 \to c_m$, whereas the coefficients of the term λ in the expressions for $\ln c_1$ in Eqs. (17a) and (17b) are required to be negative in order for $c_1 \to 0$ as $\lambda \to \infty$. That such is the case follows from the inequality $c_r \int_0^c \Psi_0 dc > \int_0^c c\Psi_0 dc$, which, in turn, follows from the fact that $(c_r - c)\Psi_0 > 0$ for $c \neq c_r$.

To examine the situation in which c_2, the larger root of Eqs. (14), approaches c_m as $\lambda \to \infty$, when $\sigma_p < \sigma_f$, we combine Eqs. (14a) and (14b) so as to eliminate terms of order of $1/(c_m - c_2)$ at $c_2 \to c_m$. Then we obtain

$$c_2[f_0'(c_2) - Z(c_2)] - [c_2 f_0'(c_1) - c_1 Z(c_1)] - \lambda \int_{c_1}^{c_2} (c_2 - c)\Psi_0 dc = 0. \qquad (18)$$

Hence, as follows from Eq. (18), the limiting value of c_1, the smaller root of Eqs. (14), depends on how the integral $\int_c^{c_m} (c_m - c')\Psi_0 dc'$ decreases with decreasing concentration c when $c < c_r$ where Ψ_0 becomes negative. As long as this integral equals zero at some concentration, say, c_1^a, Eqs. (14b) and (18) yield

$$\lambda \approx \frac{Z(c_2)}{\int_{c_1^a}^{c_m} \Psi_0 dc} \quad \text{and} \quad c_1 \approx c_1^a - \frac{c_m[f_0'(c_2) - Z(c_2)]}{\lambda(c_m - c_1^a)\Psi_0|_{c_1^a}} \qquad (19)$$

$$\text{at } c_2 \to c_m,$$

with $\int_{c_1^a}^{c_m} (c_m - c)\Psi_0 dc = 0$ and $\Psi_0|_{c_1^a} < 0$. On the other hand, $c_1 \to 0$ provided that $\int_0^{c_m} (c_m - c)\Psi_0 dc > 0$. Then we arrive at the same equations for λ and c_1 as Eqs. (17b). Furthermore, it follows from the inequality $(c - c_r)\Psi_0 > 0$, when $c \neq c_r$, that the right-hand side of the first expressions in Eqs. (19) and (17b) is positive, which is required in order that $\lambda \to \infty$ as $c_2 \to c_m$.

Now consider in more detail suspensions that are near the limit of their ability to undergo electric-field-induced aggregation, so that $c_r \to 0$ for $\sigma_p > \sigma_f$ or $c_r \to c_m$ for $\sigma_p < \sigma_f$ and for which the variation of Ψ_0 with concentration may be approximated by a linear term over the region $0 \leqslant c \leqslant c_r$ or $c_r \leqslant c \leqslant c_m$, respectively. As $c_r \to 0$, Eqs. (13) and (14) yield the following expressions: for the spinodal curve,

$$\frac{c}{c_r}\left(1 - \frac{c}{c_r}\right) \approx \frac{\lambda}{4\lambda_{cr}}$$

$$\text{with } \frac{c_{cr}}{c_r} \approx \frac{1}{2} \quad \text{and} \quad \lambda_{cr} \approx -\frac{4(1 + 4c_r)}{c_r^2 \left.\frac{\partial \Psi_0}{\partial c}\right|_{c_r}} \qquad (20a)$$

and, for the coexistence curve at $\lambda \gg \lambda_{cr}$,

$$\frac{c_2}{c_r} \approx \frac{3}{2} - \frac{\lambda_{cr}(1 + 6c_r)}{2\lambda(1 + 4c_r)} \quad \text{and} \quad \ln\left(\frac{2c_1}{3c_r}\right) \approx -\frac{4\lambda(1 + 4c_r)}{\lambda_{cr}}. \qquad (20b)$$

At the other extreme, $c_r \to c_m$, Eqs. (13) and (15) yield, for the spinodal curve,

$$\left(1 - \frac{c - c_r}{c_m - c_r}\right)^2 \left(\frac{c - c_r}{c_m - c_r}\right) \approx \frac{4\lambda_{cr}}{27\lambda} \quad \text{with}$$

$$\frac{c_{cr} - c_r}{c_m - c_r} \approx \frac{2}{3} \quad \text{and} \quad \lambda_{cr} \approx \frac{27Z''(c_r)}{8\left.\frac{\partial \Psi_0}{\partial c}\right|_{c_r}}, \qquad (21a)$$

where $Z''(c_r) \approx 2A/(c_m - c_r)^3$ [see Eq. (2b)], and for the coexistence curve at $\lambda \gg \lambda_{cr}$,

$$\frac{c_m - c_2}{c_m - c_r} \approx \frac{32\lambda_{cr}}{81\lambda} \quad \text{and} \quad \frac{c_m - c_1}{c_m - c_r} \approx \frac{3}{2} - \frac{16\lambda_{cr}}{81\lambda} \ln\left(\frac{c_m - c_2}{c_m - c_1}\right). \qquad (21b)$$

Notice that $\partial \Psi_0 / \partial c|_{c_r}$ in negative in Eqs. (20a) and positive in Eqs. (21a).

B. Classification scheme of the phase diagrams

The results of the analysis presented above demonstrate how the behavior of the spinodal and coexistence curves is related to the characteristics of the electric-field-induced long-range interparticle interactions. This yields a complete set of phase diagrams (Fig. 3) of conducting suspensions subject to dc electric fields, as a function of the mismatch of the dielectric constants and conductivities of the particles to those of the fluid. In this connection, it should be pointed out that the classification scheme of the topologies of the phase

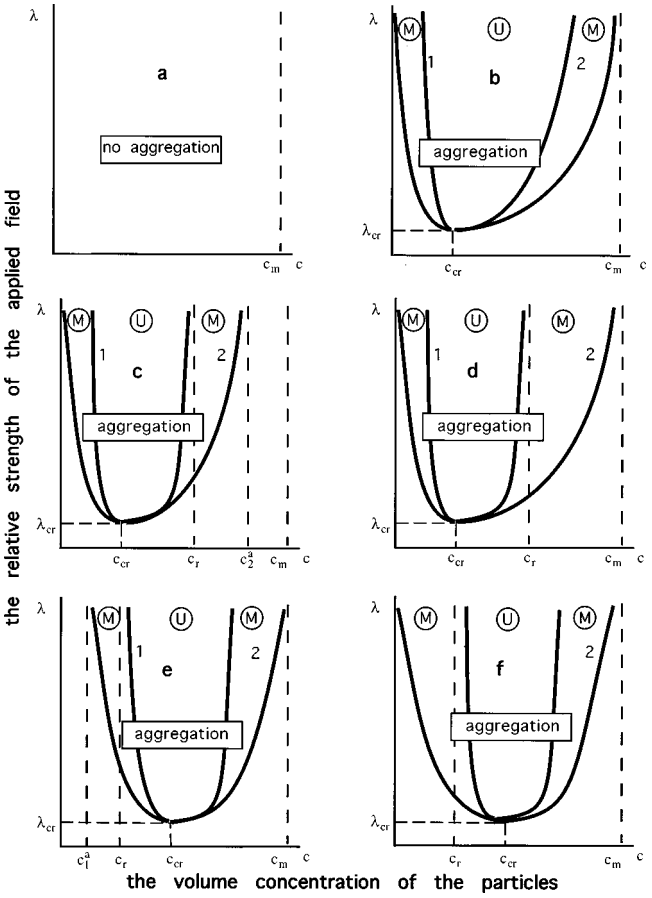

FIG. 3. Complete set of phase diagrams of conducting suspensions subject to electric fields; 1 and 2 are the spinodal and coexistence curves, respectively; the metastable and unstable domains are denoted by *M* and *U*, respectively. In the expressions, which specify the topology of a phase diagram, the subscripts 0 and ω correspond to the cases of dc and ac fields, respectively. The one-phase region of a phase diagram includes the random spatial arrangement of the particles, whereas the two-phase region corresponds to the appearance of aggregates. $\lambda=\varepsilon_f E^2 v_p/k_B T$ is a measure of the relative strength of the applied field; c is the volume concentration of the particles.

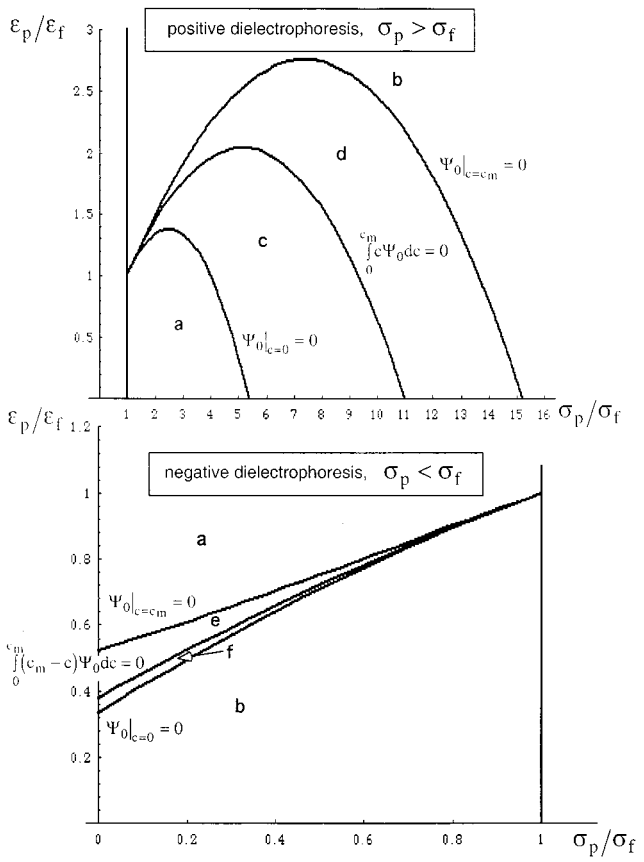

FIG. 4. Map of direct relationship between the mismatch of the dielectric constants and conductivities of particles and of a suspending fluid and the topology of the phase diagram of a conducting suspension subject to dc fields; $c_m=0.64$.

diagrams sketched in Fig. 3 is actually determined only by the asymptotic behavior of the compressibility factor $Z(c)$ as $c\to 0$ and $c\to c_m$ as well as by some rather general properties of the concentration dependence of the function Ψ_0.

The simplest phase diagram shown in Figs. 3(a) corresponds to the case when Ψ_0 is negative over the entire concentration range $0\leqslant c<c_m$, so that no aggregation at all is predicted to occur in the presence of a dc field. In contrast, the phase diagram sketched in Figs. 3(b) shows what is predicted to happen when Ψ_0 is positive for $0\leqslant c<c_m$ so that, regardless of the particle concentration, the suspension will start aggregating as long as the applied dc field becomes sufficiently large. The high-field asymptotics for the spinodal and coexistence curves on this diagram are given by Eqs. (16a), (16b), and (17b), respectively.

The diagrams depicted in Figs. 3(c) and 3(d) are encountered when $\sigma_p>\sigma_f$ and Ψ_0 changes its sign with *increasing* concentration from positive $(\Psi_0|_{c=0}>0)$ to negative $(\Psi_0|_{c=c_m}<0)$, so that it equals zero at some concentration c_r. Specifically, Fig. 3(c) applies when $\int_0^{c_2^a} c\Psi_0 dc=0$ at some c_2^a smaller than c_m, whereas, for Fig. 3(d), $\int_0^{c_m} c\Psi_0 dc>0$. The high-field behavior of the lines on the phase diagrams sketched in Figs. 3(c) and 3(d) is described by Eqs. (16a) and (16c) for the spinodal curve and by Eqs. (17a) [for Fig. 3(c)] and Eqs. (17b) [for Fig. 3(d)] for the coexistence curves. Equations (20) govern the asymptotic behavior of these curves for the phase diagram in Figs. 3(c) as $c_r\to 0$.

The phase diagrams given in Figs. 3(e) and 3(f) represent the case when $\sigma_p<\sigma_f$ and Ψ_0 changes its sign with *decreasing* concentration from positive $(\Psi_0|_{c=c_m}>0)$ to negative $(\Psi_0|_{c=0}<0)$, so that it equals zero at some concentration c_r. Figure 3(e) applies when $\int_{c_1^a}^{c_m}(c_m-c)\Psi_0 dc=0$ at some c_1^a, whereas, for Fig. 3(f), $\int_0^{c_m}(c_m-c)\Psi_0 dc>0$. The high-field asymptotics of the lines on these diagrams are described by Eqs. (16b) and (16c) for the spinodal curve and by Eqs. (19) [for Fig. 3(e)] and Eqs. (17b) [for Fig. 3(f)] for the coexistence curves. Equations (21) govern the asymptotic behavior of these lines on the phase diagram sketched in Fig. 3(e) as $c_r\to c_m$.

As can easily be shown from Eqs. (16a), (16b), (17b), and (19), the separation between the spinodal and coexistence curves along the vertical lines of constant concentrations on the phase diagram in Fig. 3(b), as well as in the low-

concentration parts of the phase diagrams in Figs. 3(c) and 3(d) and in the high-concentration parts of the phase diagrams in Figs. 3(e) and 3(f), increases indefinitely with increasing strength of the electric field.

As seen from Fig. 3, a metastable domain in the high-concentration parts of the phase diagrams in Fig. 3(c) (for $c_r<c<c_2^a$) and Fig. 3(d) (for $c_r<c<c_m$) as well as in the low-concentration parts of the phase diagrams in Fig. 3(e) (for $c_1^a<c<c_r$) and Fig. 3(f) (for $0<c<c_r$) is retained regardless of the strength of the applied dc field. Hence only the nucleation mechanisms of electric-field-induced transformations will operate in such suspensions under these conditions. However, for the phase diagram in Fig. 3(b), an increase in the electric field strength along the vertical line of constant concentration will inevitably lead to the transition from a metastable to an unstable domain at any concentration. Thus, for such suspensions, the nucleation mechanism will operate in weak fields (below the spinodal curve), whereas the spinodal decomposition will inevitably operate in strong fields (above the spinodal curve). This qualitative distinction between the transformation mechanisms should manifest itself by the dependence of the morphology of the aggregation patterns to be formed on the strength of the applied field.

The map plotted in Fig. 4 demonstrates how the topology of the phase diagram of a suspension subject to dc fields relates to the mismatch of the dielectric constants and the conductivities of the particles and those of the suspending fluid. The curves on this map were computed using Eq. (15) and the following expressions:

$$\int_0^{c_m} c\Psi_0 dc = \frac{3c_m^2\left(\frac{\sigma_p}{\sigma_f}-1\right)}{2\left[2+c_m+(1-c_m)\frac{\sigma_p}{\sigma_f}\right]^3} \times\left[6\frac{\varepsilon_p}{\varepsilon_f}-(2+c_m)-(5-2c_m)\frac{\sigma_p}{\sigma_f}+(1-c_m)\left(\frac{\sigma_p}{\sigma_f}\right)^2\right], \tag{22a}$$

$$\int_0^{c_m}(c_m-c)\Psi_0 dc = \frac{3c_m^2\left(\frac{\sigma_p}{\sigma_f}-1\right)}{2\left(2+\frac{\sigma_p}{\sigma_f}\right)^2\left[2+c_m+(1-c_m)\frac{\sigma_p}{\sigma_f}\right]^2} \times\left\{3\frac{\varepsilon_p}{\varepsilon_f}\left[4+c_m+(2-c_m)\frac{\sigma_p}{\sigma_f}\right]-2(2+c_m)-12\frac{\sigma_p}{\sigma_f}-3(1-c_m)\left(\frac{\sigma_p}{\sigma_f}\right)^2+(1-c_m)\left(\frac{\sigma_p}{\sigma_f}\right)^3\right\}. \tag{22b}$$

The domains in Fig. 4 are lettered to correspond to the phase diagrams in Fig. 3. As seen from Fig. 4, the suspension phase diagram will be given by Fig. 3(a) as the ratios σ_p/σ_f and $\varepsilon_p/\varepsilon_f$ fall within two domains, one of which is located in the region of $\sigma_p<\sigma_f$ above the curve $\Psi_0=0$ for $c=c_m$, whereas the other is in the region of $\sigma_p>\sigma_f$ below the curve $\Psi_0=0$ for $c=0$. The suspension phase diagram will be represented by Fig. 3(b) when the ratios σ_p/σ_f and $\varepsilon_p/\varepsilon_f$ fall within two other domains (Fig. 4), one of which is located below the curve $\Psi_0=0$ for $c=0$ in the region of $\sigma_p<\sigma_f$, whereas the other is above the curve $\Psi_0=0$ for $c=c_m$ in the region of $\sigma_p<\sigma_f$. On the other hand, as long as the ratios σ_p/σ_f and $\varepsilon_p/\varepsilon_f$ lie in the region of $\sigma_p>\sigma_f$ between the curves $\Psi_0=0$ for $c=c_m$ and for $c=0$, the suspension phase diagram will be represented by Figs. 3(c) and 3(d) depending on the sign of the integral $\int_0^{c_m} c\Psi_0 dc$ (Fig. 4). But if the ratios σ_p/σ_f and $\varepsilon_p/\varepsilon_f$ lie within the region of $\sigma_p<\sigma_f$ between the curves $\Psi_0=0$ for $c=c_m$ and $c=0$, the suspension phase diagram will be represented by Figs. 3(e) and 3(f) depending on the sign of the integral $\int_0^{c_m}(c_m-c)\Psi_0 dc$ (Fig. 4). Therefore, the map in Fig. 4 enables one to trace how the variations of the electrical properties of the constituent materials influence the topology of the suspension phase diagram and then, by using an appropriate diagram in Fig. 3, to evaluate how the dc-field-induced transformations depend on the strength of the applied electric field and particle concentration.

To examine the phase diagrams of conducting suspensions in more detail, we performed a numerical analysis of Eqs. (13) and (14) for the compressibility factor and the function Ψ_0 given by Eqs. (2) and (15), respectively. Figure 5 shows some representative examples showing how the parameters of the critical point λ_{cr} and c_{cr} may vary with the mismatch of the particle conductivity, σ_p/σ_f. The curves for $\varepsilon_p/\varepsilon_f=1.3$, 1.8, and 5 [Fig. 5(a)] illustrate two different types of the dependence of λ_{cr} and c_{cr} on the ratio σ_p/σ_f for the case of $\varepsilon_p/\varepsilon_f\geqslant 1$. These curves are plotted in Fig. 5(a) for $\sigma_p>\sigma_f$ since Ψ_0 is negative for $\sigma_p<\sigma_f$ as long as $\varepsilon_p/\varepsilon_f\geqslant 1$ (see Fig. 4). Such a curve [Fig. 5(a)] may consist of either one or two branches depending on whether the line $\varepsilon_p/\varepsilon_f=$const on the map in Fig. 4 passes through the domain labeled *a*. As is seen from Fig. 5(a), λ_{cr} increases without bound as the point which represents the particle-to-fluid ratios σ_p/σ_f and $\varepsilon_p/\varepsilon_f$ in Fig. 4 approaches either the line $\sigma_p=\sigma_f$ (as is the case for $\varepsilon_p/\varepsilon_f=1.3$, 1.8, and 5) or the curve $\Psi_0|_{c=0}=0$ (as occurs for $\varepsilon_p/\varepsilon_f=1.3$).

The map depicted in Fig. 4 also demonstrates that Ψ_0 can be positive for $\varepsilon_p/\varepsilon_f\leqslant 1$ only when the ratio σ_p/σ_f lies within two regions, specifically, to the right of the curve $\Psi_0|_{c=0}=0$ for $\sigma_p>\sigma_f$ and to the right of the curve $\Psi_0|_{c=c_m}=0$ for $\sigma_p<\sigma_f$. The curves for $\varepsilon_p/\varepsilon_f=0.2$, 0.38, and 0.6 plotted in Fig. 5(b) illustrate the dependence of λ_{cr} and c_{cr} on the ratio σ_p/σ_f in the case of $\varepsilon_p/\varepsilon_f\leqslant 1$ provided that $\sigma_p<\sigma_f$. In the range $\sigma_p>\sigma_f$, which lies outside of the domain labeled *a* in Fig. 4, these curves are quite similar to the corresponding branch of the curve for $\varepsilon_p/\varepsilon_f=1.3$ shown in Fig. 5(a). As can be seen from the comparison of Figs. 5(a) and 5(b) with Fig. 4 for the case $\varepsilon_p/\varepsilon_f\leqslant 1$, λ_{cr} increases without bound as the point representing the particle-to-fluid ratios σ_p/σ_f and $\varepsilon_p/\varepsilon_f$ in Fig. 4 approaches the line $\sigma_p=\sigma_f$ (as occurs for $\varepsilon_p/\varepsilon_f=0.2$, 0.38, and 0.6), the curve

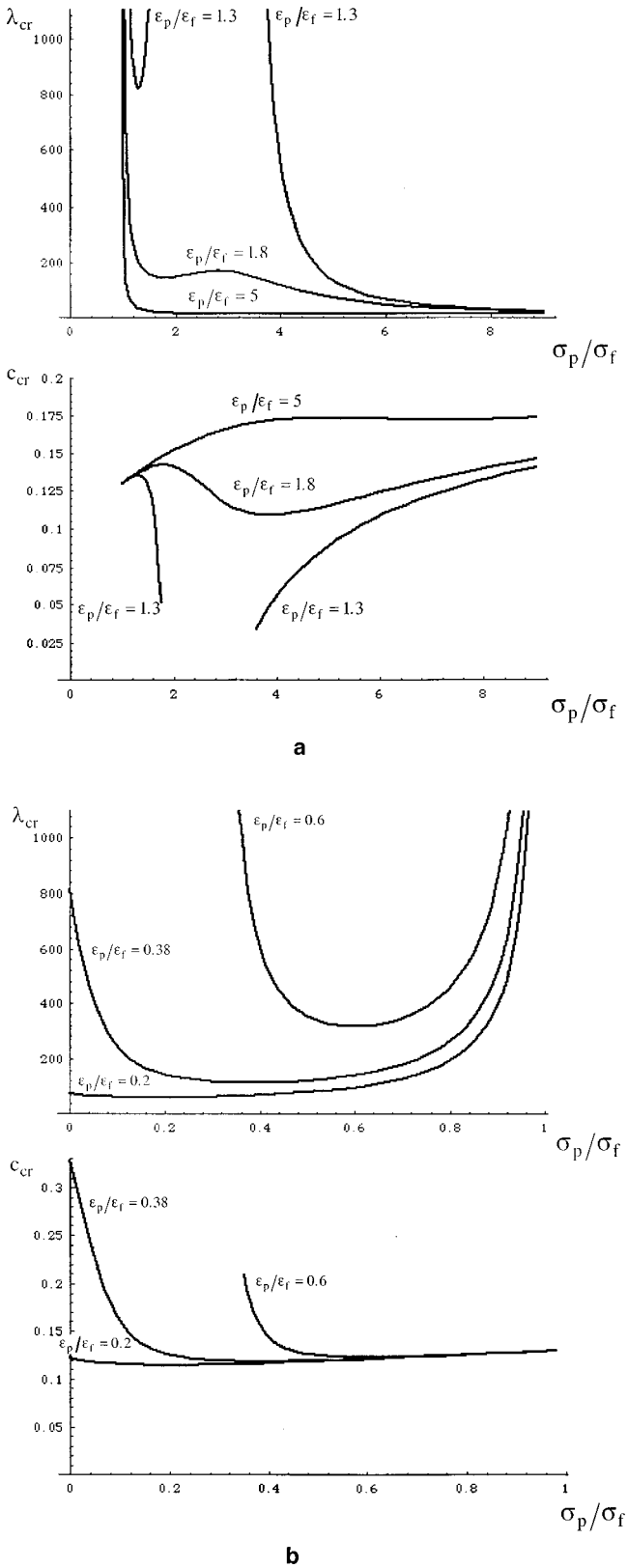

FIG. 5. Dependence of the parameters of the critical point λ_{cr} and c_{cr} on the mismatch of the particle conductivity σ_p/σ_f for (a) $\varepsilon_p/\varepsilon_f = 1.3$, 1.8, and 5 in the region of $\sigma_p > \sigma_f$ and (b) $\varepsilon_p/\varepsilon_f = 0.2$, 0.38, and 0.6 in the region of $\sigma < \sigma_f$.

$\Psi_0|_{c=c_m} = 0$ in the range of $\sigma_p < \sigma_f$ (as occurs for $\varepsilon_p/\varepsilon_f = 0.6$), or the curve $\Psi_0|_{c=0} = 0$ in the range of $\sigma_p > \sigma_f$.

Now consider the scaling properties of the suspension phase diagrams. As Fig. 5 illustrates, the values of c_{cr} and λ_{cr} vary strongly with a change in the relative particle conductivity. However, the results of numerical calculations indicate that the use of the reduced variables c/c_{cr} and λ/λ_{cr} makes it possible to superimpose the spinodal and coexistence curves in the vicinity of the critical point, approximately at $1 < \lambda/\lambda_{cr} \leqslant 2$, for a variety of the particle concentrations, electric fields, and particle properties provided that the ratios σ_p/σ_f and $\varepsilon_p/\varepsilon_f$ fall within the regions in Fig. 4 in which the topology of the suspension phase diagram does not change. Another possibility of superimposing the spinodal and coexistence curves over a variety of electric fields and particle properties, as long as Ψ_0 does not vary significantly with concentration or when the variation of Ψ_0 with concentration may be approximated by a linear term, is the use of the reduced variable λ/λ_{cr} for the strength of an electric field. For the former case, Eq. (13) reduces to that solved in Ref. [1], so that $c_{cr} \approx 0.13$ and $\lambda_{cr}\Psi_0 \approx 21.20$ when Ψ_0 is positive. For example, this case is associated with the parts of the curves plotted in Fig. 5(a) for $\sigma_p/\sigma_f \leqslant 2$ and in Fig. 5(b) for $0.5 \leqslant \sigma_p/\sigma_f$. The other situation corresponds to the phase diagrams depicted in Figs. 3(c) and 3(e). Under these circumstances, the use of the reduced variable for the concentration, namely, $(c-c_r)/c_{\text{width}}$ with c_{width} being the width of the two-phase region, makes it possible to superimpose the spinodal and coexistence curves over a variety of the concentrations as well. This result correlates well with the pertinent asymptotic expressions, namely, Eqs. (20) with $c_{\text{width}} = 3c_r/2$ and Eqs. (21) with $c_{\text{width}} = 3(c_m - c_r)/2$. Another important case is that of highly conducting particles, so that $\sigma_p/\sigma_f \to \infty$ and $6\varepsilon_p/\varepsilon_f \ll (\sigma_p/\sigma_f)^2$; then, Eq. (15) yields $\Psi_0 \to 3/(1-c)^3$. Under these conditions, the suspension phase diagram corresponds to Fig. 3(b) with $c_{cr} \to 0.27$ and $\lambda_{cr} \to 3.89$. This limiting case correlates well, for example, with the behavior of the curves in Fig. 5(a) at sufficiently large values of σ_p/σ_f.

It should be pointed out that the value of the particle content, c_2, of the high-concentration phase of a suspension in the phase diagrams in Fig. 3 increases dramatically with the strength of the applied field. For example, c_2 approaches ~ 0.5 at $\lambda/\lambda_{cr} \sim 2$ for the phase diagram plotted in Fig. 3(b). This value almost corresponds to a transition from a disordered state to an ordered face-centered-cubic structure on the equilibrium phase diagram of hard spheres in the absence of an electric field [3,4]. In this connection, we also mention recent studies of suspensions of nonconducting particles in nonconducting fluids subject to strong electric fields [12] which demonstrate that a high-concentrated phase in such colloids eventually forms a crystalline body-centered tetragonal solid. Thus it is quite realistic to suppose that a high-concentration phase in the diagrams in Fig. 3 should undergo subsequent disorder-to-order transitions in the presence of sufficiently strong electric fields as well. Unfortunately, a description of these transformations cannot be included in the diagrams in Fig. 3 because of the absence of an equation for the free energy of conducting anisotropic crystalline aggregates, which is required for this analysis.

IV. PHASE DIAGRAMS OF SUSPENSIONS SUBJECT TO ac FIELDS

Algebraic and numerical operations in this section were performed with the use of MATHEMATICA [13].

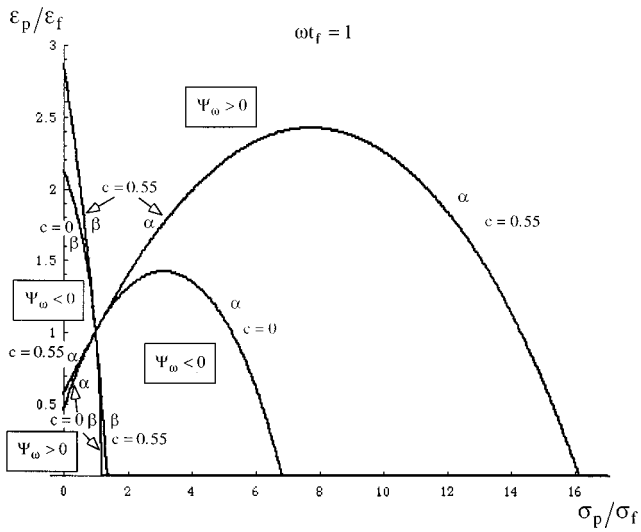

FIG. 6. Family of curves $\Psi_\omega(\varepsilon_p/\varepsilon_f, \sigma_p/\sigma_f, \omega t_f, c)=0$ in the σ_p/σ_f and $\varepsilon_p/\varepsilon_f$ plane for $\omega t_f=1$ on $c=0$ and 0.55. $\Psi_\omega(\varepsilon_p/\varepsilon_f, \sigma_p/\sigma_f, \omega t_f, c)$ is positive in two domains, one of which is located above the β curve in the region of $\sigma_p \leqslant \sigma_f$ and above the α curve in the region of $\sigma_p > \sigma_f$, whereas the other is located below the α curve in the region of $\sigma_p \leqslant \sigma_f$ and below the β curve in the region of $\sigma_p > \sigma_f$.

When a suspension is subjected to an ac electric field $E_0 \cos \omega t$ over a long period of time ($t \gg t_s$), the substitution of Eqs. (5) for its electric energy into Eqs. (9) and (11) yields expressions similar to those in Eqs. (13) and (14) with

$$\Psi_\omega\left(\frac{\varepsilon_p}{\varepsilon_f}, \frac{\sigma_p}{\sigma_f}, \omega t_f, c\right) = \frac{\partial^2}{\partial c^2}\left(\frac{W}{\varepsilon_f \langle E\rangle_T^2}\right) \tag{23}$$

in place of Ψ_0 and $\lambda = \varepsilon_f \langle E\rangle_T^2 \nu_p / k_B T$, where $\langle E\rangle_T^2 = E_0^2/2$ is the time average of the square of the electric field strength, and $t_f = \varepsilon_f/\sigma_f$ is the time constant of the fluid. The nondimensional function Ψ_ω represents the time average energy of the long-range interparticle interactions under ac fields, and the value of λ is a measure of the relative strength of the applied ac electric field; in addition, $\Psi_\omega \to \Psi_0$ as $\omega t_f \to 0$.

Reasoning similar to that in Sec. III A shows that a curve $\Psi_\omega(\varepsilon_p/\varepsilon_f, \sigma_p/\sigma_f, \omega t_f, c)=0$ in the σ_p/σ_f and $\varepsilon_p/\varepsilon_f$ plane represents a boundary between a domain where the particle properties are such that these particles will aggregate in the presence of a sufficiently strong ac electric field (since, for them, $\Psi_\omega > 0$) and a domain where they will not aggregate (since, for them, $\Psi_\omega < 0$). Figure 6 depicts a family of such curves for different values of the particle concentration. As seen from Fig. 6, there exist two different curves for every value of c; both of them go through the point $\sigma_p/\sigma_f = \varepsilon_p/\varepsilon_f = 1$ and intersect the axes. With $\omega t_f \to 0$, the curve labeled α approaches the corresponding curve for a dc field (see Fig. 2), which is given by the equation $\Psi_0(\varepsilon_p/\varepsilon_f, \sigma_p/\sigma_f, c)=0$ at $\sigma_p \neq \sigma_f$, whereas the curve labeled β approaches the line $\sigma_p = \sigma_f$, so that it intersects the axes at the points

$$\frac{\sigma_p}{\sigma_f} \approx 1 + \frac{1+3c}{6}\omega t_f \quad \text{and} \quad \frac{\varepsilon_p}{\varepsilon_f} \approx \left[\frac{X_\beta(c)}{\omega t_f}\right]^{1/2} \quad \text{as} \quad \omega t_f \to 0, \tag{24a}$$

with $X_\beta(c)$ being the positive root of the equation

$$(2-3c+c^3)X_\beta^2 + (4-15c+c^3)X_\beta - 16 - 12c + c^3 = 0.$$

On the other hand, as $\omega t_f \to \infty$, the α and β curves approach the line $\varepsilon_p = \varepsilon_f$ at any finite value of σ_p/σ_f, while the points where they intersect the axis $\varepsilon_p/\varepsilon_f = 0$ approach infinity according to

$$\frac{\sigma_p}{\sigma_f} \approx \left[\frac{\omega t_f}{Y_{\alpha,\beta}(c)}\right]^{1/2} \quad \text{at} \quad \omega t_f \to \infty, \tag{24b}$$

with Y_α and Y_β being the only two positive roots ($Y_\alpha < Y_\beta$, respectively) of the cubic equation

$$2(2+c)^3 Y^3 - 3(8+c)(2+c)(1-c)Y^2 - 9(1+2c)(1-c)Y + (1-c)^3 = 0.$$

The sign of $\delta(\varepsilon_p/\varepsilon_f)/\delta c|_{\sigma_p/\sigma_f, \omega t_f, \Psi_\omega = 0}$, which shows how $\varepsilon_p/\varepsilon_f$ varies with concentration for the curves α and β along the lines $\sigma_p/\sigma_f = \text{const} \neq 1$, is always positive. Therefore, as can be seen from Fig. 6, a necessary condition for a conducting suspension to undergo a phase transition in the presence of an ac field is that the particle-to-fluid ratios of the dielectric constants and conductivities should lead to either $\Psi_\omega(\varepsilon_p/\varepsilon_f, \sigma_p/\sigma_f, \omega t_f, 0) > 0$ or $\Psi_\omega(\varepsilon_p/\varepsilon_f, \sigma_p/\sigma_f, \omega t_f, c_m) > 0$. If in addition, however, Ψ_ω changes sign at some concentration, say c_r, so that $\Psi_\omega(\varepsilon_p/\varepsilon_f, \sigma_p/\sigma_f, \omega t_f, c_r)=0$, then the spinodal curve will appear on the suspension phase diagram in the range $0 < c < c_r$ or $c_r < c < c_m$, respectively. In a manner similar to that in Sec. III A, we can show that the asymptotic behavior of the spinodal and coexistence curves at strong electric fields when $\lambda \to \infty$ is given by Eqs. (16), (17), and (19)–(21) with Ψ_ω in place of Ψ_0. As a result, Fig. 3 also yields a complete set of phase diagrams of conducting suspensions subject to an ac electric field as a function of the mismatch of the dielectric constants and conductivities of the particles and suspending fluid as well as of the frequency of the applied field.

The map plotted in Fig. 7(a) [see Fig. 7(b) for an enlargement of the left-hand side corner of Fig. 7(a), i.e., for $0 \leqslant \varepsilon_p/\varepsilon_f \leqslant 2$ and $0 \leqslant \sigma_p/\sigma_f \leqslant 3$] demonstrates how the topology of the phase diagram of a suspension subject to ac fields relates to the mismatch of the dielectric constants and conductivities of particles and a suspending fluid for $\omega t_f = 5$. The domains in this map are lettered to correspond to the phase diagrams in Fig. 3. As seen from Fig. 7, the suspension phase diagram will be given by Fig. 3(a) when the ratios σ_p/σ_f and $\varepsilon_p/\varepsilon_f$ fall within two domains, one of which is located in the region of $\sigma_p < \sigma_f$ bounded by the β curve for $c=0$ and the α curve for $c=c_m$, whereas the other is located in the region of $\sigma_p > \sigma_f$ bounded by the α curve for $c=0$ and the β curve for $c=c_m$. The suspension phase diagram will be represented by Fig. 3(b) when the σ_p/σ_f and $\varepsilon_p/\varepsilon_f$ ratios fall within another two domains (Fig. 7), one of which is located above the β curve for $c=c_m$ in the region of $\sigma_p < \sigma_f$ and above the α curve for $c=c_m$ in the region of $\sigma_p \geqslant \sigma_f$, whereas the other is located below the α curve for $c=0$ in the region of $\sigma_p < \sigma_f$ and below the β curve for $c=0$ in the region of $\sigma_p \geqslant \sigma_f$. As long as the ratios σ_p/σ_f and $\varepsilon_p/\varepsilon_f$ lie within the region of $\sigma_p < \sigma_f$ between the β

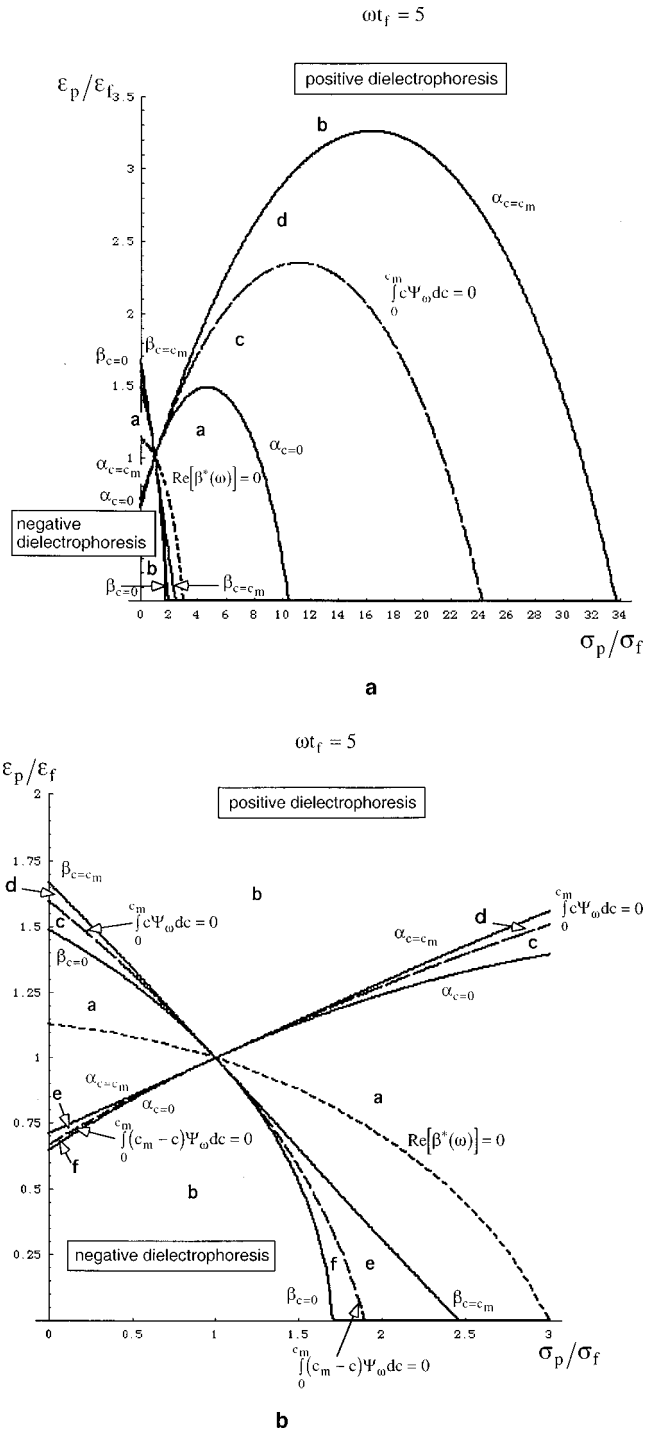

FIG. 7. Map of the direct relationship between the mismatch of the dielectric constants and conductivities of particles and of a suspending fluid and the topology of the phase diagram of a conducting suspension subject to ac fields for $\omega t_f=5$ and $c_m=0.64$. (b) Enlargement of the left-hand-side corner ($0\leqslant\varepsilon_p/\varepsilon_f\leqslant 2$, $0\leqslant\sigma_p/\sigma_f\leqslant 3$) of the map.

curves for $c=c_m$ and $c=0$, as well as within the region of $\sigma_p\geqslant\sigma_f$ between the α curves for $c=c_m$ and $c=0$, the suspension phase diagram will be represented by Figs. 3(c) and 3(d) depending on the sign of the integral $\int_0^{c_m} c\Psi_\omega dc$. On the other hand, if the ratios σ_p/σ_f and $\varepsilon_p/\varepsilon_f$ lie within the region of $\sigma_p<\sigma_f$ between the α curves for $c=c_m$ and $c=0$, as well as within the region of $\sigma_p\geqslant\sigma_f$ between the β curves for $c=c_m$ and $c=0$, the suspension phase diagram will be represented by Figs. 3(e) and 3(f) depending on the sign of the integral $\int_0^{c_m}(c_m-c)\Psi_\omega dc$.

The map plotted in Figs. 7(a) and 7(b) enables one to trace how the variations of the electrical properties of the constituent materials influence the topology of the suspension phase diagram and then, by using an appropriate diagram in Fig. 3, to evaluate how the electric-field-induced transformations will depend on the strength of an ac field and the particle concentration. To this end, it is significant to examine how Ψ_ω varies with increasing the field frequency. As follows from Eqs. (12b) and (23), $\Psi_\omega\rightarrow\Psi_\omega=3\beta^2/(1-\beta c)^3>0$ as $\omega t_f\rightarrow\infty$. Therefore, at $\varepsilon_p\neq\varepsilon_f$ and regardless of the ratio σ_p/σ_f, the suspension phase diagram will eventually correspond to Fig. 2(b) as the field frequency becomes sufficiently high. The parameters of the critical point λ_{cr} and c_{cr} for this limiting case were calculated in Ref. [2]; note that this λ_{cr} equals $\Lambda_{cr}/3\beta^2$ in the notation of Ref. [2]. The dependence of Λ_{cr} and c_{cr} on β is plotted in Fig. 1 of Ref. [2]. An increase in β from $\beta=-0.5$ to $\beta=1$ leads to a decrease in Λ_{cr} from 25.24 to 11.66 and to an increase in c_{cr} from 0.11 to 0.27; $\Lambda_{cr}\rightarrow 21.20$ and $c_{cr}\rightarrow 0.13$ as $\beta\rightarrow 0$ [2], so that $\lambda_{cr}\rightarrow\infty$ as $\beta\rightarrow 0$.

Depending on the values of the ratios σ_p/σ_f and $\varepsilon_p/\varepsilon_f$ as well as the particle concentration, Ψ_ω may either increase or decrease monotonically with ωt_f from Ψ_0 to Ψ_∞, or may attain a minimum or a maximum at an intermediate frequency. Moreover, this minimum may be negative even when Ψ_0 is positive. In this interesting case, the suspension phase diagram will correspond to Fig. 3(b) at low frequencies, then to Fig. 3(a) within some frequency range (so that these particles do not aggregate in such ac electric fields), and then again to Fig. 3(b) at sufficiently high frequencies. As an example, a map of possible forms of the frequency dependence of Ψ_ω for $c\rightarrow 0$ in the σ_p/σ_f and $\varepsilon_p/\varepsilon_f$ plane is plotted in Fig. 4 of Ref. [1].

Now consider how an increase in the frequency of an ac electric field affects the two subdomains in Figs. 7(a) and 7(b) within which Ψ_ω is negative. Specifically, as ωt_f increases, the domain *a* located in the region $\sigma_p<\sigma_f$ shrinks to the line $\varepsilon_p=\varepsilon_f$, so that it disappears gradually as $\omega t_f\rightarrow\infty$. On the other hand, the domain *a* located in the region $\sigma_p>\sigma_f$ and bounded by the β curve for $c=c_m$ and the α curve for $c=0$ [Figs. 7(a) and 7(b)] is retained. These boundaries move indefinitely to the right as $\omega t_f\rightarrow\infty$ and, moreover, the separation between them along the lines $\varepsilon_p/\varepsilon_f=$const increases. For example, this behavior can be seen from Eqs. (24b) for the points of the intersection of the curves α and β with the axis $\varepsilon_p/\varepsilon_f=0$. Within a part of the domain $\sigma_p>\sigma_f$ through which these boundaries traverse, the sign of Ψ_ω will vary with frequency from positive to negative and then again to positive. This demonstrates why Ψ_ω should always become positive at any fixed values of the ratios σ_p/σ_f and $\varepsilon_p/\varepsilon_f$ as the field frequency is made sufficiently high.

V. COMBINED EFFECTS OF DIELECTROPHORESIS AND AGGREGATION

The term *dielectrophoresis* is used to describe the electric-field-induced motion of electrically uncharged par-

ticles in spatially nonuniform electric fields [5,8,9]. The dielectrophoretic force experienced by a single spherical conducting particle immersed in a conducting fluid under a slightly nonuniform electric field $\mathbf{e}(\mathbf{r},t)$ can be expressed as [2,9]

$$\mathbf{F}_D(\mathbf{r},t)=3v_p\varepsilon_f\left(\left[\int_0^t B(t-t')\mathbf{e}(\mathbf{r},t')dt'\right]\cdot\nabla\right)\mathbf{e}(\mathbf{r},t), \tag{25a}$$

where

$$B(t)=\frac{\varepsilon_p-\varepsilon_f}{\varepsilon_p+2\varepsilon_f}\delta(t)+\frac{3(\varepsilon_f\sigma_p-\varepsilon_p\sigma_f)}{(\varepsilon_p+2\varepsilon_f)^2}\exp\left(-\frac{t}{t_p}\right)$$

with $t_p=(\varepsilon_p+2\varepsilon_f)/(\sigma_p+2\sigma_f)$ being the relaxation time for the charge redistribution at the particle surface, $\delta(t)$ is the delta function, and $\mathbf{e}$ is the electric field acting on this particle. The integral term in Eq. (25a) represents the relative dipole strength of this particle.

With a cell model, we can generalize Eq. (25a) so as to get an equation for a dielectrophoretic force exerted on a test particle in a concentrated suspension subject to a nonuniform electric field $\mathbf{E}(\mathbf{r},t)$. For this purpose, the average field acting on a particle $\mathbf{e}$ should be not the applied field $\mathbf{E}$, but the Lorentz-Lorenz local field which is related to $\mathbf{E}$ by (see Sec. IV A in Ref. [1])

$$\mathbf{E}(\mathbf{r},t)=\mathbf{e}(\mathbf{r},t)-c\int_0^t B(t-t')\mathbf{e}(\mathbf{r},t')dt'. \tag{25b}$$

By taking the Laplace or Fourier transforms of Eq. (25b), we can express the local field $\mathbf{e}$ in terms of $\mathbf{E}$ and, after inverting the transform, eliminate $\mathbf{e}$ from Eq. (25a). But since this procedure is rather lengthy, we shall consider only the cases of a suspension subjected to a dc field $E(\mathbf{r})$ or to an ac field $E_0(\mathbf{r})\cos\omega t$ over a long period of time ($t\gg t_s$). For a dc electric field, we obtain that

$$\mathbf{F}_D=\frac{3}{2}v_p\varepsilon_f\frac{\dfrac{\sigma_p-\sigma_f}{\sigma_p+2\sigma_f}}{\left(1-c\dfrac{\sigma_p-\sigma_f}{\sigma_p+2\sigma_f}\right)^2}\nabla E^2. \tag{26a}$$

On the other hand, for an ac electric field, Eqs. (25) yield an expression for the dielectrophoretic force as an oscillating function of time whose time average is

$$\langle\mathbf{F}_D\rangle_T=\frac{3}{2}v_p\varepsilon_f\frac{\mathrm{Re}[\beta^*(\omega)]}{|1-c\beta^*(\omega)|^2}\nabla\langle E\rangle_T^2$$

$$\text{with}\quad \beta^*(\omega)=\frac{\varepsilon_p^*(\omega)-\varepsilon_f^*(\omega)}{\varepsilon_p^*(\omega)+2\varepsilon_f^*(\omega)}. \tag{26b}$$

Note that

$$\beta^*(\omega)\to\frac{\sigma_p-\sigma_f}{\sigma_p+2\sigma_f}\quad\text{as}\quad\omega t_f\to 0$$

$$\text{and}\quad\beta^*(\omega)\to\frac{\varepsilon_p-\varepsilon_f}{\varepsilon_p+2\varepsilon_f}\quad\text{as}\quad\omega t_f\to\infty.$$

hence, Eq. (26b) includes Eq. (26a) as a limiting case. The nominators in Eq. (26) represent the dielectrophoretic force acting on a single particle [8,9], whereas denominators account for the effect of the other particles on the magnitude of the force exerted on a test particle in a suspension.

Now consider how a spatial nonuniformity of an electric field can contribute to aggregation phenomena in a conducting suspension. As follows from Eqs. (26), the application of such a field will induce a spatial rearrangement of the particles which will be attracted toward high-field regions (positive dielectrophoresis [8,9]) when $\mathrm{Re}[\beta^*(\omega)]>0$ ($\sigma_p>\sigma_f$ for a dc field) and to low-field regions (negative dielectrophoresis [8,9]) when $\mathrm{Re}[\beta^*(\omega)]<0$ ($\sigma_p<\sigma_f$ for a dc field). It is convenient to represent the spatial variations of the local values of the particle concentration, $c(\mathbf{r},t)$, and of the strength of an electric field, $E(\mathbf{r},t)$, by a trajectory (c as a function of E) on the suspension phase diagram which is given by one of the diagrams in Fig. 3. With increasing electric field strength along this trajectory, the particle concentration should be increasing for positive and decreasing for negative dielectrophoresis, respectively. These trajectories will correspond to the lines of equal chemical potential when the particles reach their quasiequilibrium spatial arrangement in a nonuniform electric field [2]. As long as such a trajectory passes through a two-phase domain in the suspension phase diagram, aggregation is predicted to occur in an associated portion of this suspension, so that dielectrophoresis will be accompanied by an electric-field-induced phase transition. The limiting case of a nonconducting suspension is examined in Ref. [2] in more detail.

The curve $\mathrm{Re}[\beta^*(\omega)]=0$ plotted on the maps in Figs. 4 and 7 delineates the different regimes of dielectrophoresis (the region of negative dielectrophoresis contains the origin $\sigma_p/\sigma_f=\varepsilon_p/\varepsilon_f=0$). It is significant that this curve lies in the interior of the domains *a* in Figs. 7(a) and 7(b) and, as $\omega t_f\to 0$, coincides with the boundary between the domains *a* and *b* for a dc field (Fig. 4). Hence the domains *e* and *f* and the domains *c* and *d* in Figs. 4 and 7 are associated with different regimes of dielectrophoresis, negative and positive, respectively. The maps in Figs. 4 and 7 enable one to trace how the properties of the constituent materials influence the electric-field-induced aggregation and dielectrophoresis in a suspension subjected to a nonuniform electric field. For example, dielectrophoresis cannot be accompanied by aggregation if a point representing the particle properties lies within domain *a* in Figs. 4 and 7.

VI. DISCUSSION AND COMPARISON WITH EXPERIMENTAL DATA

One of the main conclusions of our theory is that there are points of similarity between the phase diagrams of ''the particle concentration vs the electric field strength'' and the concentration vs temperature phase diagrams for the first-order phase separation in quenched conventional binary systems with a high-temperature miscibility gap (Fig. 3). Specifically, as can be seen from the phase diagrams in Fig. 3, our theory predicts that the process of phase separation in a suspension can be characterized by two critical values of the field strength, E_{c1} and E_{c2}. The smaller critical field E_{c1} corresponds to the intersection, on the phase diagram, between the

vertical passing through the concentration c of the particles in this suspension and the coexistence curve, whereas the greater field E_{c2} refers to the intersection of the same vertical with the spinodal curve. Accordingly, this suspension is predicted to remain homogeneous as long as the applied electric fields are lower than E_{c1}, while, slightly above E_{c1}, randomly distributed particles will start forming high-concentration domains that are separated from one another. Nucleation then plays an important role in the range from E_{c1} to E_{c2}, whereas spinodal decomposition prevails at fields larger than E_{c2}. As we shall see, this framework offers a convincing explanation as to why a diverse set of colloids being exposed to sufficiently strong electric fields exhibits similar aggregation patterns.

Phase transformations in suspensions of electrically neutral particles under the action of strong electric fields were studied experimentally in electrorheological (ER) fluids and in some aqueous suspensions related to biomedical applications. An ER fluid is a suspension of highly polarized micrometer-sized particles dispersed in low-conducting oils. The electrically induced particle aggregation in an ER fluid manifests itself in a quick and dramatic reversible increase in the apparent suspension viscosity following the application of an electric field. References [14–19] provide a good introduction to the field of ER fluids.

Some uncertainty in attempting to make a quantitative comparison between the theoretical predictions and the published experimental data lies in the fact that, in the experiments involving suspensions subject to strong electric fields, the numerical values of the mismatch of the effective conductivities of the particles and suspending fluid, σ_p/σ_f, were not well defined. Recall, that the addition of a small amount of ionic impurities to low conducting liquids and solids can radically alter their conductivity. Therefore, the values of the conductivities of the particles and suspending fluid in a suspension could differ by an order of magnitude from those of the pure substances. Unfortunately, in spite of considerable efforts to link the electrical properties of the particulate phase to the ER response, only a few investigations attempted to characterize the conductivity of the disperse phase [20,21]. In addition, the Maxwell-Wagner model of interface polarization, which underlies our theory, requires some modifications related to modeling the charge transfer inside the double layer on the particle surface in order to provide a correct interpretation of the experimental data pertaining to the low-frequency complex permittivity for many colloids, even in the case of low fields [4,7].

Nevertheless, as will be seen below, we are able to demonstrate how the available experimental data on the electric-field-driven phase separation in a variety of suspensions can be interpreted within the context of our theory and why the currently used models of the field-induced aggregation are not capable of providing a unifying framework for explaining this body of experimental results.

A. Experimental data and their interpretation by our theory

Two different regimes of an electric-field-driven separation in colloids, whose appearance depends on the strength of the applied field as predicted by the phase diagrams in Fig. 3, were observed in ER fluids in Ref. [22]. These authors studied the separation of a quiescent homogeneous layer of an ER fluid into high-concentration and low-concentration domains under the action of a transverse dc electric field. Experiments were performed on a 20–vol % suspension of diatomite particles (radius about 1 μm) dispersed in a transformer oil ($\varepsilon_f/\varepsilon_0 \sim 2.2$ and $\varepsilon_p/\varepsilon_f \sim 1.2-1.8$), and the structural transformations were observed in the plane perpendicular to the electric field. It was found that the suspension remained homogeneous for applied fields less than $E_{c1}=1.41$ kV/mm, but as the field strength exceeded this threshold value, the homogeneous suspension rearranged itself into a system of separated high-concentration domains surrounded by a low-concentration phase. This structure indicates that the phase separation was created via the nucleation of a new phase, the characteristic length scale of which increased exponentially with increasing field strength. At $E_{c2}=1.86$ kV/mm and beyond, the morphology of the suspension layer changed again in that the high-concentration domains formed an interconnected sievelike structure similar to that commonly observed in quenched conventional binary systems as long as the spinodal mechanism prevails in the first-order phase transition. For the suspension employed in Ref. [22], the magnitudes of the ratio of the electric energy to the thermal energy calculated for the critical fields 1.41 and 1.86 kV/mm are $\lambda_{c1} \approx 3.9 \times 10^4$ and $\lambda_{c2} \approx 6.8 \times 10^4$, respectively. As can be seen from Fig. 5, such large values of λ_{c1} and λ_{c2} correspond to a small mismatch of the conductivities of the particles and fluid $(\sigma_p - \sigma_f)/\sigma_f \ll 1$ when $\Psi_0(\varepsilon_p/\varepsilon_f, \sigma_p/\sigma_f, c) \to 0$. This is consistent with the fact that the suspension employed in Ref. [22] was not activated with special polar additives used in electrorheology [15,18,19] in order to increase the particle conductivity.

Experimental data presented in Refs. [23–26] show the relation between the morphology of the aggregation patterns formed in a suspension under the action of a dc field and the mismatch of the dielectric constants and conductivities of the particles and fluid. In Refs. [23–26], the structure of a quiescent layer of a suspension was observed, again in the direction perpendicular to the field lines, and experiments were performed on model ER fluids consisting of a wide variety of particulates dispersed in silicone oil ($\varepsilon_f/\varepsilon_0 \sim 2.6$ [27]). Specifically, the particles used in Refs. [23–26] were microspheres of copper and indium (metal), silicon (semiconductor, $\varepsilon_p/\varepsilon_f \sim 4.5$ [27]), strontium titanate (low conductivity and high dielectric constant, $\varepsilon_p/\varepsilon_f \sim 50-300$ [27]), PMMA (very low conductivity and low dielectric constant, $\varepsilon_p/\varepsilon_f \sim 0.85$ [27]), and glass (low conductivity and $\varepsilon_p/\varepsilon_f \sim 1.4$ [27]) as well as Cu spheres coated with an insulating layer of SiO_2, PMMA spheres coated with a monolayer of Ni or a double layer of Ni and SiO_2, glass spheres coated with a layer of Ni (~ 1.5 μm thickness) or a double layer of Ni and insulating lead zirconic titanate (PZT) ceramics (~ 1 μm thickness), and glass spheres containing some amount of absorbed water. In Refs. [23,24] the diameters of the copper, silicon, and $SrTiO_3$ spheres were about 40 μm, while those of the indium, PMMA, and glass spheres were about 25, 70, and 45 μm, respectively. In Refs. [25,26] the diameters of the copper, $SrTiO_3$ spheres, and glass spheres were about 65, 10, and 47 μm, respectively. The particle volume fraction of indium particles was 0.2, whereas the volume fractions in all

other suspensions were in the range 0.05–0.10. Unfortunately, these authors did not measure the particle conductivity. Aggregation patterns were observed for spatially uniform electric fields in the range 0.5–0.7 kV/mm. Under these conditions and for the particle sizes referred to above, the electric-energy–to–thermal energy ratio is $\lambda_{expt} \sim 10^8$. In addition, field-induced aggregation patterns were observed in spatially nonuniform electric fields over a similar range of electric field strengths generated by needle-needle, needle-plate, and concentric cylindrical electrodes [25,26].

In the presence of an electric field, the $SrTiO_3$ and Si spheres formed a system of separated chainlike aggregates aligned in the direction of the field lines as is typically observed in ER fluids [14–19]. However, the aggregates formed by the Si spheres were significantly greater in length than those formed by the $SrTiO_3$ spheres under the action of the same strength of the applied field. On the other hand, the morphology of the aggregation patterns observed in suspensions of copper and indium spheres subjected to a dc electric field was completely different from that in suspensions of $SrTiO_3$ and silicon spheres in that these metallic particles formed a netlike (also referred to as fractal) structure. But when the copper spheres were coated with an insulating layer of SiO_2, the aggregation patterns were found to be similar to those formed in a suspension of $SrTiO_3$ particles.

Another interesting phenomenon was observed in suspensions with PMMA and glass spheres. In the absence of coating, the PMMA particles did not aggregate at all, but when these same spheres were coated with a very thin nickel layer, short chainlike separated aggregates were formed which were aligned in the direction of the field lines. When, however, the thickness of the nickel layer was increased so as to form a uniform conducting layer, the PMMA particles formed netlike aggregation patterns similar to those formed by metallic spheres. If this outer nickel layer on the PMMA spheres was then covered with an insulating layer of SiO_2, short chainlike aggregates appeared again. Similarly, for glass spheres, the structure of the aggregation patterns was radically altered as the amount of water absorbed by the particles was increased or as they were coated with either only conducting (Ni) material or sequentially with conducting (Ni) and insulating (PZT) materials. Specifically, at relatively low water content (up to about 1 wt %), the glass spheres formed chainlike separated aggregates whose length increased with the amount of absorbed water. However, when the water content exceeded several percent, the aggregates became shorter and more branchy. On further increasing the amount of water (more that about 5 wt %), the suspension structure became similar to the netlike aggregation patterns observed in suspensions of metallic particles. The netlike aggregation structure also appeared when the glass spheres were coated with a conducting nickel layer. However, this netlike pattern transformed back to chains when an insulating PZT layer was coated over the Ni layer. Experiments in Refs. [25, 26] showed that the spatial nonuniformity of electric fields does not affect the morphology of the particle aggregation patterns.

The experimental data reported in Refs. [23–26] fit naturally into the scheme in Fig. 4, which demonstrates how the aggregation processes in dc fields depend on the mismatch of the dielectric constants and conductivities of the particles to those of the suspending fluid. In particular, suspensions of copper and indium particles fall in the region of large values of σ_p/σ_f in Fig. 4 and their phase diagram is represented by Fig. 3(b) with values of λ_{cr} being at least of $O(10^2)$ as can be seen from Fig. 5(a). Hence, for suspensions of metallic particles, the experimental conditions of Refs. [23–26] corresponded to the regime $\lambda_{expt} \gg \lambda_{cr}$, which, in the phase diagram, we associate with the unstable domain lying far beyond the spinodal curve. This is consistent with the experimental results that these suspensions formed netlike aggregation patterns similar to the structures observed in quenched binary systems when the spinodal mechanism plays the main role in the phase separation.

Even though a detailed analysis of a suspension with composite particles is beyond the present scope of our theory, the scheme in Fig. 4 also readily explains why the coating of the PMMA particles with nickel affected their ability to aggregate in the presence of a dc electric field. Specifically, without coating, the parameters of the PMMA suspension fell within domains in Fig. 4 where the suspension phase diagram is given by Fig. 3(a), so that no aggregation would be expected to occur. As can be seen from Fig. 4 for $\varepsilon_p/\varepsilon_f \sim 0.85$, in order for the PMMA particles to aggregate in dc fields it is required that the value of the ratio σ_p/σ_f should lie in the range either from 1 to about 4.5 or less than about 0.7. This argument is consistent with the low-conducting properties of the PMMA materials. On the other hand, covering a particle with a thick nickel layer led to a large value of the ratio σ_p/σ_f with σ_p being taken as the effective conductivity of a composite particle. Hence the parameters of this suspension fell into the region in Fig. 4 related to the phase diagram given by Fig. 3(b) with relatively small values of λ_{cr} (see Fig. 5). This means that the strength of the applied electric fields in these experiments fell within the unstable part of the suspension phase diagram, far beyond the spinodal curve. As a result, a suspension of the PMMA spheres coated with a thick nickel layer formed netlike aggregation patterns very similar to those in suspensions of metallic particles. To this end, it is quite reasonable to expect that the cases of PMMA particles coated with a very thin Ni layer or double layer coated with an inner thick Ni layer and an outer insulating SiO_2 layer were associated with the region of moderate values of σ_p/σ_f in Fig. 4. Such σ_p/σ_f ratios correspond to the phase diagrams given by Figs. 3(b), 3(c), or 3(d) with sufficiently large values of λ_{cr} (see Fig. 5). Consequently, according to our model, the value of λ_{expt} for such suspensions was associated with the metastable domain between the coexistence and spinodal curves in the suspension phase diagram. As could be expected for this domain, a suspension should form a system of separated aggregates similar to structures observed in quenched binary systems when nucleation plays an important role in the phase separation. Such is indeed the structure observed in experiments with PMMA particles coated with a thin Ni layer or double layer coated with Ni and SiO_2 layers.

The impact of absorbed water and coating with nickel on the aggregation patterns of glass spheres in the presence of a dc electric field observed in Refs. [23–26] provides further support for our proposed model. Recall that, as follows from Fig. 4 for $\varepsilon_p/\varepsilon_f \sim 1.4$, the value of the ratio σ_p/σ_f is required to be greater than unity for glass particles to aggregate

in dc fields. But the water content of glass spheres in Refs. [23, 24] was varied in the same range as that of traditional water-activated ER fluids where, as has been well established in experiments with such ER fluids [15–19], the conductivity of similar dispersed particles (glass, silica, quartz, aluminum and magnesium silicate, zeolite, etc.) increases drastically with the amount of absorbed water. Consequently, it appears reasonable to suppose that the value of λ_{expt} was associated with the unstable domain in the suspension phase diagram for highly watered glass spheres (large σ_p/σ_f ratios) and with the metastable one for particles with relatively small water content (moderate σ_p/σ_f values). As a result, highly watered particles formed netlike aggregation patterns, whereas particles containing small amount of water formed a system of separated aggregates. This argument is consistent with the experimental result that highly watered glass particles formed a structure similar to the netlike structure observed in suspensions of glass particles covered with a conducting nickel layer for which, as one would expect, the σ_p/σ_f ratio was large.

The same reason readily explains why the coating of copper spheres with an insulating layer of SiO_2 as well as the coating of the nickel layer on the glass spheres with an insulating PZT layer (a double coating) caused a radical change in the morphology of the dc-field-driven aggregation patterns. This is because the effective ratio σ_p/σ_f was drastically reduced due to the coating, so that λ_{expt} fell into the metastable domain in the suspension phase diagram. As a result, phase separation in suspensions made of coated copper particles and double-coated glass spheres occurred mainly via the nucleation mechanism, leading to the formation of a system of separated aggregates.

Similarly, if silicon and strontium titanate particles are to aggregate in dc fields, the value of the ratio σ_p/σ_f should be greater than unity (Fig. 4). As one could expect, the values of the ratio σ_p/σ_f for these particles were significantly lower than those of metallic particles; hence, the value of λ_{expt} was associated with the metastable domain in their phase diagrams. Consequently, these particles formed separated aggregates under the action of a dc field. The fact that the aggregates of silicon particles were greater in size than those of the $SrTiO_3$ particles may be attributed to the larger conductivity of silicon, leading to a smaller value of λ_{cr} compared with that for strontium titanate particles. This, in turn, leads to a larger value of $\lambda_{expt}/\lambda_{cr}$ for the silicon particles, thereby resulting in a larger ''supersaturation'' (i.e., the distance from the coexistence curve in the phase diagram) which ''drives'' the field-induced phase separation.

The experimental result [25,26] that a spatial nonuniformity of the electric field (on the scale larger than the particle size) does not influence the morphology of the field-induced aggregation patterns demonstrates that the driving force for aggregation is determined by the *local* strength of the electric field. This correlates well with our model [1,2] in that the driving force for aggregation arises from the field-induced interparticle interactions (governed by the local field strength), whereas the spatial nonuniformity of the field affects spatial variations in the particle concentration.

It is significant that our theory predicts that the similarities in field-driven phase separation processes in suspensions are associated with the same type of phase diagrams of ''the particle concentration vs the electric field strength'' in Fig. 3. All the experiments discussed above, though, were conducted in suspensions where the ratio $\varepsilon_p/\varepsilon_f$ was greater than approximately 0.85.

In relation to the behavior of suspensions with small values of $\varepsilon_p/\varepsilon_f$ and σ_p/σ_f, it is pertinent to mention the experiments of Refs. [28,29] on the ac-field-induced aggregation of polystyrene ($\varepsilon_p/\varepsilon_0 \sim 2.5$) spheres (diameter of 1.3–1.5 μm) suspended in an aqueous medium and confined to a thin layer. The properties of these suspensions were located in the vicinity of the origin of the coordinates ($\varepsilon_p/\varepsilon_f \ll 1$ and $\sigma_p/\sigma_f \ll 1$) of Figs. 4 and 7, and therefore their phase diagrams refer to those plotted in Fig. 3(b). In Ref. [28], 30- and 150-kHz fields of 0.1–0.13 kV/mm were applied to a 0.9–vol % suspension in the plane of the layer, whereas in Ref. [29] a 1.5-kHz field of 0.03 kV/mm was applied transversely to a layer of a 0.12–vol % suspension. The strength of the applied fields in these experiments corresponded to λ_{expt} equal to approximately 1.7×10^3 and 2.5×10^3 in Ref. [28] and 300 in Ref. [29].

As was observed in Refs. [28,29], polystyrene spheres formed separated chainlike aggregates aligned in the direction of the field lines. These resembled the structures typical of ER fluids which are also related to the phase diagram in Fig. 3(b), however, for $\varepsilon_p/\varepsilon_f \geqslant 1$ and $\sigma_p/\sigma_f \geqslant 1$. The similarity between the structure formation in these suspensions is consistent with what would have been expected from the similarities between their phase diagrams. It should be noted, however, that as shown in Ref. [30] the Maxwell-Wagner model should be modified by including a frequency-dependent surface admittance in order to account for the observed low-field complex dielectric permittivity of an aqueous suspension of polystyrene spheres. Therefore, a more detailed analysis of the phase diagram of polystyrene suspensions is beyond the present scope of our theory.

In relation to the expected ability of suspensions, having small values of the ratio $\varepsilon_p/\varepsilon_f$, to undergo spinodal decomposition, it might be well to point out Refs. [31,32]. These authors reported the results of light-scattering studies of the structure formation in transparent suspensions (5–17 vol %) of silica spheres (diameter of 0.7 μm) in 4-methylcyclohexanol ($\varepsilon_f/\varepsilon_0 \sim 13.5$ and $\varepsilon_p/\varepsilon_f \sim 0.3$) subject to 12-kHz electric fields $\sim$0.8–3 kV/mm. The measurements of the depolarization of the scattered light indicated that these particles were sufficient refractive-index matched to the suspending fluid so as to ensure single scattering from a suspension. Light-scattering data taken within milliseconds after the application of an electric field showed two distinct lobes orthogonal to the field lines. These lobes had an intensity maximum at some nonzero wave vector, indicating a strong spatial correlation between unstable concentration fluctuations. These authors [31,32] emphasized that this scattering pattern was the two-dimensional analog of the scattering ring commonly observed in the spinodal decomposition of quenched conventional binary systems which are isotropic. Moreover, a typical scattering ring was observed when the light beam was directed along the field lines. The fact that the silica suspensions in the experiments of Refs. [31,32] showed the field-induced spinodal decomposition is consistent with the predictions of our theory. Specifically, the conditions of these experiments corresponded to values

of the electric energy-to-thermal energy ratio λ_{expt} from approximately 3.3×10^3 to 4.5×10^4. As can be seen from Fig. 5 for $\varepsilon_p/\varepsilon_f\sim0.3$, these values of λ_{expt} far exceeded λ_{cr} for a dc field and, consequently, λ_{cr} for ac fields since the latter decreases with increasing field frequency when $\varepsilon_p/\varepsilon_f<1$.

One of the important theoretical predictions of our model is that the field-induced phase separation can occur in suspensions associated with positive as well as negative regimes of dielectrophoresis in Figs. 4 and 7. In other words, the ability of particles to aggregate in the presence of a spatially *uniform* electric field is not related to the sign of the dielectrophoretic force acting on them in a spatially *nonuniform* field. This statement correlates well with, for example, the observed similarities between the structure formation in aqueous suspensions of polystyrene spheres [28,29] and in ER fluids [23–26] discussed above. Those suspensions were associated with the domains of negative and positive dielectrophoresis in Figs. 4 and 7, respectively. Data on the electric-field-induced scattering dichroism in suspensions [33] provide more support for this view. In Ref. [33] experiments were performed on concentrated (15–40 vol %) suspensions of silicon dioxide spheres (sizes from 0.092 to 0.7 μm) subject to dc electric fields up to 1 kV/mm. The particles were refractive-index matched to a suspending fluid. Specifically, particles smaller than 0.2 μm were suspended in cyclohexane ($\varepsilon_f/\varepsilon_0\sim2$) or cyclohexane with a small amount of decalin. Those particles exhibited positive dielectrophoresis. Larger particles were suspended in a mixed solvent of toluene ($\varepsilon_f/\varepsilon_0\sim2.4$) and ethanol ($\varepsilon_f/\varepsilon_0\sim24$). For them, the sign of the dielectrophoretic force was negative. Measurements of the time variation of the dichroism following the application and removal of the electric field provided evidence that the imposition of an electric field ($\lambda_{expt}\sim6$–200) on these suspensions caused the particles to form an anisotropic structure. These measurements [33] indicated that, regardless of the sign of the dielectrophoretic force, all their suspensions showed similar trends as concerns the dependence of the field-induced dichroism on the particle concentration and field strength, even though the time scale for relaxation increased monotonically with particle size.

The maps plotted in Figs. 4 and 7 show that the application of electric fields can cause a suspension to undergo phase separation only on condition that the ratios σ_p/σ_f and $\varepsilon_p/\varepsilon_f$ fall outside the domains associated with the phase diagram in Fig. 3(a). In particular, Fig. 4 predicts that particles dispersed in a fluid having a smaller dielectric constant than that of the particles ($\varepsilon_f<\varepsilon_p$) will not aggregate in dc fields if their conductivities are smaller than that of the fluid ($\sigma_p<\sigma_f$). Such particles will aggregate, however, if their conductivity is increased to the point where it becomes larger than that of the fluid due to absorption of small amounts of a polar liquid (water, for example) or the addition of some ionic dopants. It is interesting to note that a theory for dilute suspensions [1] leads to the same prediction. As was already discussed in Ref. [1], data on the dc-field-induced structure formation in ER fluids consisting of humidified cornstarch in corn oil [20] provide support for this view. Specifically, these experiments showed that cornstarch formed chainlike structures for water contents greater than 3 wt %, but incomplete chains and partial alignment of the particles at lower water contents. For the purpose of the applicability of our model, it is significant that the dried cornstarch had a larger dielectric constant and a smaller conductivity than the corn oil, but that the cornstarch conductivity increased rapidly with the amount of absorbed water, so that it became larger than the oil conductivity at water contents greater than 3 wt %. This result correlates well with the requirement that, in order for particles having $\varepsilon_p>\varepsilon_f$ to aggregate, the value of the ratio σ_p/σ_f should exceed unity (Fig. 4).

Recently published data on ER responses in a model emulsion system [21] also substantiate the predictions which follow from Fig. 4. Here, two immiscible fluids, a chlorinated paraffin oil ($\varepsilon_{ch}/\varepsilon_0\sim8.1$, $\sigma_{ch}\sim10^{-9}$ S/m) and a silicone oil ($\varepsilon_s/\varepsilon_0\sim2.7$, $\sigma_s\sim10^{-12}$ S/m), were used to prepare the emulsions. Those having 10 and 20 vol % silicone oil consisted of silicone oil droplets dispersed in the paraffin oil. At silicone volume fractions 30% and above, the emulsions consisted of paraffin oil droplets dispersed in the silicone oil. Their structure formation was observed, however, only in thin layers of 10% and 90% emulsions, to which a dc field was applied in the plane of a sample. In both emulsions and in the absence of the electric field, droplets of the dispersed phase were found to be randomly distributed within the continuous matrix. But immediately following the application of an electric field of 5 kV/mm to the 10% emulsion, the droplets of silicone oil formed chainlike aggregates aligned along the field lines. These aggregates were not stable under static conditions, however, in that they disappeared gradually due to the existence of field-induced fluid motions in the sample and, as time elapsed, also coalesced. In contrast, after applying a dc field of 4 kV/mm to the 90% emulsion, paraffin oil droplets formed stable slender ''warmlike'' liquid columns, mainly oriented along field lines. Although the experiments of Ref. [21] indicated significant complications in field-driven processes in emulsions, as compared with that in suspensions, arguments based on the map in Fig. 4 can explain the sharp contrast between the structure formation in these emulsions.

The conditions of the experiments reported in Ref. [21] corresponded to values of the electric energy-to-thermal energy ratio λ_{expt} equal to approximately 1.8×10^6 for the 10% emulsion and 3.9×10^5 for the 90% emulsion. The former was associated with the ratios $\varepsilon_p/\varepsilon_f\sim0.33$ and $\sigma_p/\sigma_f\sim10^{-3}$, whereas the latter with the ratios $\varepsilon_p/\varepsilon_f\sim3$ and $\sigma_p/\sigma_f\sim10^3$. The values of the dielectric relaxation time t_s for these emulsions were ~0.01 s. For short times $t\ll t_s$, the electric energy of both emulsions was determined by the ratio $\varepsilon_p/\varepsilon_f$ [see Eqs. (4a) and (12b)], so that the droplets started aggregating as soon as the dc field was applied since λ_{expt} far exceeded the high-frequency limit $\lambda_{cr}=\Lambda_{cr}/3\beta^2$ (see Sec. IV) equal to approximately 270 and 160 for the 10% and 90% emulsions, respectively. However, the stability of the structure in the long-time limit $t\gg t_s$ involved the ratio of the conductivities as well. For these emulsions, the ratios $\varepsilon_p/\varepsilon_f$ and σ_p/σ_f fell within different domains in Fig. 4 related to the phase diagram in Fig. 3(b). Specifically, the point of the 10% emulsion was located near the upper boundary of the left domain, whereas the point of the 90% emulsion was located inside the right domain far away from its boundaries. Hence this explains why both emulsions underwent a dc-field-induced structure formation and why the long-term stability of the 10% emulsion under static conditions was sig-

nificantly lower. It might be well to point out that the possibility of the scenario which was observed in Ref. [21] for the 10% emulsion, namely, that a structure formed immediately ($t \ll t_s$) after the application of a dc field can become unstable in the long-time limit, was predicted in Ref. [1].

Field-induced formation of chainlike aggregates was also observed in aqueous emulsions and suspensions of biological cells, erythrocytes, potato starch, ion-exchange resins, fat globules, etc. [34–38], over a range of frequencies and field strengths. The frequency dependence of the dielectric constant and the conductivity of these systems exhibit more than single dielectric dispersions, which in turn, requires modification of the Maxwell-Wagner model in order to represent the experimental data. Hence one might expect that the phase diagrams of such colloids could be significantly richer than those plotted in Fig. 3. Even so, our theory appears to be able to justify Schwan's semiempirical relation between the particle size R and threshold strength of an ac field, E_{th}, required to cause aqueous dispersions to aggregate [36,37]:

$$E_{\mathrm{th}} R^{1.5} = K. \tag{27}$$

Schwan then showed [36,37] that by choosing a value of K on the right-hand side of Eq. (27) lying in the range $6.6 \times 10^{-6} - 11 \times 10^{-6}\ \mathrm{V\,m^{1/2}}$, it is possible to fit the experimental data on chain aggregation in aqueous suspensions of silicon particles (low polarized) and various biological cells (highly polarized) for particle sizes from ~ 1 to $\sim 100\ \mu\mathrm{m}$. Schwan proposed Eq. (27) based on the assumption that, for the onset of a chain formation, the energy of a polarized particle subject to an external electric field should equal the thermal energy [36].

But as can be seen from the phase diagrams in Fig. 3, λ_{cr} gives the lowest value of the electric energy-to-thermal energy causing phase separation and that the ac field strength $E_{0\mathrm{cr}}$ associated with λ_{cr} is [see Eq. (23)]

$$E_{0\mathrm{cr}} R^{3/2} = \left(\frac{3 \lambda_{\mathrm{cr}} k_B T}{2 \pi \varepsilon_f} \right)^{1/2}. \tag{28}$$

With $T = 300\ \mathrm{K}$, $\varepsilon_f / \varepsilon_0 = 78$, and the limiting values of λ_{cr} equal to 33.6 for low ($\varepsilon_p / \varepsilon_f \ll 1$ and $\sigma_p / \sigma_f \ll 1$) and 3.9 for highly ($\sigma_p / \sigma_f \gg 1$) polarized particles (see Secs. III and IV), we obtain that the right-hand side of Eq. (28) falls within the range between 3.4×10^{-6} and $9.8 \times 10^{-6}\ \mathrm{V\,m^{1/2}}$ in reasonably good agreement with the value of K in Eq. (27) proposed by Shwan. Therefore, Eq. (28) can be used for obtaining a rough estimate of the smaller critical field E_{c1} above which particles will start aggregating, except for very dilute or for highly concentrated suspensions since, in that case, the value of E_{c1} varies drastically with concentration (see the coexistence curves in the phase diagrams in Fig. 3).

Although our theory does not deal with the rheology of ER fluids, it provides some insight into the major trends of the ER response. Recall that field-induced shear stresses in ER fluids depend on the interaction between nearly touching particles [17–19], whereas our model considers primarily long-range interparticle interactions represented by $\Psi_0(\varepsilon_p/\varepsilon_f, \sigma_p/\sigma_f, c)$ [see Eq. (15)] for dc fields and $\Psi_\omega(\varepsilon_p/\varepsilon_f, \sigma_p/\sigma_f, \omega t_f, c)$ [see Eq. (23)] for ac fields. Nevertheless, one might expect a correlation between field-induced shear stresses and long-range interparticle interactions. Based on this assumption, we can link the ER response to these functions Ψ_0 and Ψ_ω. For example, our model for a dilute suspension in Ref. [1] that gave Ψ_0 and Ψ_ω at $c = 0$ clarified the reasons why the ER activity of a suspension correlates with its dielectric spectrum and why the yield shear stresses increase initially with an increase in the ratio σ_p / σ_f up to a maximum and then decrease as was first reported in Ref. [18]. Also, it was predicted that, depending on the values of the ratios $\varepsilon_p / \varepsilon_f$ and σ_p / σ_f, the function $\Psi_\omega|_{c=0}$ can decrease or increase monotonically or even vary nonmonotonically with increasing field frequency ωt_f. All these results remain unchanged in the case of a concentrated suspension. Thus our theory provides a natural interpretation of the general trend found in the literature on ER fluids [16–19,39–42] that, with increasing field frequency, it is possible to observe either a monotonically decreasing, a monotonically increasing, or a nonmonotonically varying ER response.

In connection with the frequency dependence of Ψ_ω, we recall the fact (see Sec. IV) that domain a located in the region $\sigma_p > \sigma_f$ [Figs. 7(a) and 7(b)] is retained in ac fields with its boundaries moving indefinitely to the right as $\omega t_f \to \infty$. This peculiarity provides a natural interpretation of the observation that, in many ER fluids, the ER response drops drastically within some narrow frequency range. The phenomenon of the drastic drop in the ER response was first reported in Ref. [43] and, since then, has been considered mostly as an artifact because no reasonable explanation could be provided. According to our model, however, such a drop in the ER response of a suspension can be related to frequencies when domain a passes either through or near the point $\varepsilon_p / \varepsilon_f$ and σ_p / σ_f, which represents the properties of this suspension in Fig. 7. At these frequencies, the values of Ψ_ω and, correspondingly, the ER response decrease dramatically.

B. Drawbacks of currently available models for electric-field-induced aggregation in suspensions

Two basic models have been used to interpret the tendency of a group of neutral particles to form chainlike aggregates aligned in the direction of the electric lines [8,9,14–19,34–38]. One of them is related to the well-known equation for the dipole-dipole energy W_{dd} [5] between two nonconducting spheres immersed far apart in a nonconducting fluid:

$$W_{dd} = 3 \varepsilon_f E^2 v_p \beta^2 \left(\frac{a}{R} \right)^3 (1 - 3 \cos^2 \theta) \quad \text{with} \quad \beta = \frac{\varepsilon_p - \varepsilon_f}{\varepsilon_p + 2 \varepsilon_f}, \tag{29}$$

where a is the particle radius, R is the distance between their centers, and θ is the angle between their line of centers and the direction of electric field. Two polarized spheres clearly attract each other, irrespective of the sign of β, as long as $\cos^2 \theta > 1/3$, in particular, when their line of centers is parallel to the electric field. On the other hand, they repel each other if $\cos^2 \theta < 1/3$, in particular, when their line of centers is

perpendicular to the electric field. Numerous theoretical papers exploit modifications of this model for computer modeling of aggregation phenomena in ER fluids [12,14,16]. In general terms, this model is similar to the de Gennes–Pincus model [44] for aggregation phenomena in colloids of ferromagnetic grains.

The other interpretation of field-induced particle interactions is based on the distortion of the applied electric field in the vicinity of each particle, which leads to a dielectrophoretic force acting on another particle (see Sec. V). For a nonconducting sphere immersed in a nonconducting fluid, the field is intensified near the poles and reduced near the equator when $\beta>0$, while the reverse occurs when $\beta<0$. The dielectrophoretic force acting on a nonconducting sphere is [see [5] or Eq. (25a)]

$$\mathbf{F}_D=\frac{3}{2}v_p\varepsilon_f\beta\boldsymbol{\nabla}E^2. \tag{30}$$

Since the dielectrophoretic force drives a particle towards the high-field regions for $\beta>0$ and towards the low-field regions for $\beta<0$, we find that two particles aligned parallel or perpendicular to the electric field will attract or repel each other, correspondingly. Hence the tendency of the particle motion derived from Eq. (30) is consistent with that following from Eq. (29).

The core assumption in both these models is that the particles and fluid are treated as nonconducting and hence these models are referred to as electrostatic [16,18,19]. They predict that, as the strength of an applied electric field becomes sufficiently large, particles having a dielectric constant different from that of the suspending fluid, so that $\beta\neq0$, will aggregate. In addition, as can be seen from Eqs. (29) and (30) the field-induced interparticle interactions should be an increasing function of the mismatch of the dielectric constants of the particles and fluid. However, as has been widely discussed in the literature [16,18,19], the predictions of electrostatic models often contradict many of the experimental data on ER fluids. As an example, we can mention that suspensions of barium titanate particles, where $\varepsilon_p/\varepsilon_0\approx1600$, give a weak ER performance, which, however, can be significantly improved when the particles absorb a small amount of water [16]. Also, the predictions of the electrostatic model are inconsistent with the experimental results discussed in Sec. VI A according to which PMMA spheres did not aggregate without the presence of metallic coating even though $\beta\neq0$ and that silicon particles ($\beta\approx0.3$) formed aggregates longer in size than those formed by $SrTiO_3$ spheres ($\beta\geqslant0.9$) [23].

Recent attempts to generalize the electrostatic polarization model in order to include the effects of conductivity employ the Maxwell-Wagner model [9,16]. Specifically, they either use the expression for the dielectrophoretic force acting on a conducting sphere or attempt to include the complex particle dipole coefficient $\beta^*(\omega)$ into Eq. (29) for the dipole-dipole energy.

The equation for the dielectrophoretic force for the Maxwell-Wagner model [9],

$$\mathbf{F}_D=\frac{3}{2}v_p\varepsilon_f\,\mathrm{Re}[\beta^*(\omega)]\boldsymbol{\nabla}\langle E\rangle_T^2, \tag{31}$$

can be obtained by replacing β in Eq. (30) by $\mathrm{Re}[\beta^*(\omega)]$ [see Eq. (26b)]. The force-based models which employ Eq. (31) show that the ability of the particles to aggregate under the action of strong electric fields depends on the mismatch not only in dielectric constants, but also in the conductivity between the particles and fluid. Specifically, for the particles to aggregate under the action of low-frequency fields, it is required that their conductivity be different from that of the fluid (so that $\sigma_p\neq\sigma_f$), whereas for high-frequency fields a mismatch in dielectric constant is required (so that $\varepsilon_p\neq\varepsilon_f$) [see Eq. (26b) as $\omega t_f\rightarrow0$ and $\omega t_f\rightarrow\infty$, respectively]. Although this model is superior to the electrostatic one, its predictions are still at variance with many of the experimental results discussed in Sec. VI A. In particular, the prediction that the dc-field-induced interparticle interactions are increasing functions of the mismatch in the conductivity is in contradiction with the fact that the yield shear stresses of ER fluids increase initially with an increase in the ratio σ_p/σ_f up to a maximum and then decrease [18]. Also, this force-based model is unable to explain why PMAA spheres with metallic coating ($\sigma_p>\sigma_f$, positive dielectrophoresis) did aggregate under the action of a dc field, whereas the same spheres without metallic coating ($\sigma_p<\sigma_f$, negative dielectrophoresis) did not aggregate [23]. In fact, this model predicts that the PMMA particles should aggregate irrespective of the coating since their conductivity in both cases was different from that of the suspending fluid. Any further attempts to improve the force-based model by accounting for the sign of the dielectrophoresis will contradict the observations of Ref. [33] that the ability of particles to aggregate is independent of the sign of the dielectrophoretic force.

Now let us consider the energy-based models. Those which are commonly used in the literature (for example, [8,36,37,45]) employ a rather arbitrary modification of the equation for the energy of the dipole-dipole interaction of two conducting spheres. Specifically, by using an analogy with the transformation of Eq. (30) into Eq. (31), they replace β^2 in Eq. (29) with either $|\beta^*(\omega)|^2$ or $|\mathrm{Re}[\beta^*(\omega)]|^2$. Although such equations include the mismatch in the dielectric constants as well as in the conductivities between the particles and fluid, their predictions are still at variance with many of the experimental results discussed in Sec. VI A. For instance, since [see Eq. (26b)]

$$|\beta^*(\omega)|^2,|\mathrm{Re}[\beta^*(\omega)]|^2\rightarrow\left(\frac{\sigma_p-\sigma_f}{\sigma_p+2\sigma_f}\right)^2 \quad \text{as} \quad \omega t_f\rightarrow0,$$

they predict that the particles having the conductivity different from that of the fluid (so that $\sigma_p\neq\sigma_f$) will aggregate under the action of low-frequency fields. This result is in contradiction with the experimental observations mentioned above that PMAA spheres with metallic coating ($\sigma_p>\sigma_f$) did aggregate under the action of a dc field, whereas the same spheres without metallic coating ($\sigma_p<\sigma_f$) did not aggregate [23].

In Ref. [1] we performed rigorous calculations of the electric energy of two conducting spheres and the surrounding conducting fluid for the Maxwell-Wagner model. As was shown in Ref. [1] (see Sec. III D), the dipole-dipole energy W_{dd} of these spheres, being subjected to (i) a dc field E for short and long times and (ii) an ac field $E_0\cos\omega t$ over a long

period of time, is given by the following expressions, respectively: (i) for a dc electric field,

$$W_{dd}=3\varepsilon_f E^2 v_p \Psi^d(t)\left(\frac{a}{R}\right)^2(1-3\cos^2\theta), \qquad (32)$$

with $\Psi^d(t)\to\beta^2$ as $t\ll t_p$ and $\Psi^d(t)\to\Psi_0|_{c=0}$ as $t\gg t_p$, where $t_p=(\varepsilon_p+2\varepsilon_f)/(\sigma_p+2\sigma_f)$ is the relaxation time of the interfacial polarization and $\Psi_0|_{c=0}$ is given by Eq. (15) at $c=0$, and (ii) for an ac electric field,

$$W_{dd}=\frac{3}{2}\varepsilon_f v_p E_0^2\langle\Psi^d(t)\rangle\Big|_T\left(\frac{a}{R}\right)^2(1-3\cos^2\theta), \qquad (33)$$

where $\langle\Psi^d(t)\rangle|_T=\Psi_\omega|_{c=0}$ is the time average of $\Psi^d(t)$ as $t\gg t_p$ with $\Psi_\omega|_{c=0}$ given by Eq. (23) at $c=0$.

On comparing Eq. (29) with Eqs. (32) and (33), we see that as $t\gg t_p$, the effect of the interfacial polarization on the particle interaction is reflected by the difference between the values of the coefficient β^2 for nonconducting particles and those of $\Psi_0|_{c=0}$ and $\Psi_\omega|_{c=0}$ for conducting particles. Hence Eqs. (32) and (33) predict that the application of a sufficiently strong dc and ac electric fields will cause the particles to aggregate as long as $\Psi_0|_{c=0}$ and $\Psi_\omega|_{c=0}$ are positive. As a result, these predictions are in fact equivalent to those given by the maps in Figs. 4 and 7 for the limiting case of dilute suspensions as $c\to 0$. The validity of these predictions was discussed in Sec. IV A.

An attempt to perform computer simulations of the field-induced fractal pattern formation of metal particles in an insulating fluid was undertaken in Ref. [46]. The model proposed in Ref. [46] considers the two-dimensional motion of polarized particles subject solely to the forces exerted by a spatially nonuniform external electric field and by the fluid [i.e., the dielectrophoretic force, Eq. (30), and the Stokes drag force acting on a single particle]. This model ignores the field-induced interactions between the polarized particles, their hard-core interactions, and the Brownian forces as well as the difference between the local effective field acting on a particle and the external field caused by the presence of other dipoles. As a result of these assumptions, this model predicts, for example, that the application of a uniform electric field would cause no motion or aggregation of the particles. This prediction is in contradiction with the fact [25,26] that the spatial nonuniformity of the applied electric field does not influence the morphology of the field-induced aggregation patterns observed in suspensions.

VII. CONCLUSIONS

We developed a theory for the phase diagrams of ''the particle concentration vs the electric field strength'' for electric-field-induced phase transitions in concentrated colloids of electrically neutral spheres. The main obstacle which had to be overcome in constructing a theory was that the electric energy density of conducting suspensions cannot be constructed using Brillouin's formula given by macroscopic electrodynamics [5,6] since this formula is applicable only under the severe limitations of negligibly small conductivity effects. To overcome these limitations of Brillouin's formula, we developed a microscopic theory for the electric energy density of conducting spheres randomly dispersed in a conducting fluid provided that the particles and fluid can be described by the model of a leaky dielectric [1,2]. This model corresponds to the classical mechanism of the Maxwell-Wagner interfacial polarization typical of colloids [7–9].

One of the main predictions of our theory is that there are points of similarity between the phase diagrams of conducting colloids subject to dc and ac electric fields and the concentration vs temperature phase diagrams for the first-order phase separation in quenched conventional binary systems with a high-temperature miscibility gap (Fig. 3). As a result, the process of field-induced phase separation in a suspension can be characterized by two critical values of the field strength, E_{c1} and E_{c2}, depending on the particle concentration. We predict that the particles will be randomly distributed as long as the applied electric fields are lower than E_{c1}. On the other hand, in the range from E_{c1} to E_{c2}, nucleation of high-concentration domains that are separated from one another is predicted to play the major role, whereas spinodal decomposition of a suspension prevails at fields larger than E_{c2}. This explains why a diverse set of colloids being exposed to strong electric fields exhibits similar aggregation patterns.

We demonstrated that our theory offers a convincing interpretation of the available experimental data on aggregation phenomena in electrorheological fluids and aqueous suspensions under the action of strong electric fields. Then we showed that currently used energy- and force-based theoretical models are in variance with many of these experimental results, so that they are unable to provide a unifying framework for interpreting this body of data.

In summary, our theory enables one to trace how the variations of the electrical properties of the constituent materials influence the topology of the suspension phase diagram of ''the particle concentration vs the electric field strength'' and then to evaluate the effects of the field strength and frequency on the particle aggregation.

ACKNOWLEDGMENTS

This work was supported in part by grants from the National Science Foundation (No. CTS-974475) and the National Aeronautics and Space Administration (No. NCC3-607) and by the State of New York under its Einstein Chair Program.

[1] B. Khusid and A. Acrivos, Phys. Rev. E **52**, 1669 (1995).
[2] B. Khusid and A. Acrivos, Phys. Rev. E **54**, 5428 (1996).
[3] A. K. Sood, in *Solid State Physics*, edited by H. Ehrenreich and D. Turnbull (Academic, San Diego, CA, 1991), Vol. 45, pp. 2–73.
[4] W. B. Russel, D. A. Saville, and W. R. Schowalter, *Colloidal Dispersions* (Cambridge University Press, Cambridge, England, 1989), Chap. 10.
[5] L. D. Landau, L. P. Lifshitz, and L. P. Pitaevskii, *Electrodynamics of Continuous Media* (Pergamon, Oxford, 1984), Chap.

II and IX.
[6] L. Brillouin, *Wave Propagation and Group Velocity* (Academic, New York, 1960), Chap. IV.
[7] S. S. Dukhin and V. N. Shilov, *Dielectric Phenomena and the Double Layer in Disperse Systems and Polyelectrolytes* (Wiley, New York, 1974).
[8] H. A. Pohl, *Dielectrophoresis: The Behavior of Neutral Matter in Nonuniform Electric Fields* (Cambridge University Press, Cambridge, England, 1978).
[9] T. B. Jones, *Electromechanics of Particles* (Cambridge University Press, Cambridge, England, 1995).
[10] L. D. Landau and L. P. Lifshitz, *Statistical Physics* (Pergamon, Oxford, 1980), Pt. 1.
[11] Recent review of phase transitions in conventional atomic systems can be found in J. S. Langer, in *Systems Far from Equilibrium*, edited by L. Garrido, *Lecture Notes in Physics* Vol. 132 (Springer-Verlag, Berlin, 1980), pp. 12–47; K. Binder, *ibid.* pp. 76–90; (Springer-Verlag, Berlin, 1980); J. D. Gunton, in *Statistical and Particle Physics: Common Problems and Techniques*, edited by K. C. Bowler and A. J. McKane (Scottish Universities Summer School in Physics, Edinburgh: The School, 1983), Vol. 26, pp. 101–153; J. D. Gunton, M. San Miguel, and P. S. Sahni, in *Phase Transitions and Critical Phenomena*, edited by C. Domb and J. L. Lebowitz (Academic, London, 1983), Vol. 8, pp. 269–466; K. F. Kelton, in *Solid State Physics*, edited by H. Ehrenreich and D. Turnbull (Academic, San Diego, CA, 1991), Vol. 45, pp. 75–177.
[12] Recent theoretical analysis of phase transitions in nonconducting suspensions can be found in R. Tao and J. M. Sun, Phys. Rev. Lett. **67**, 398 (1991); R. Tao and Qi Jiang, *ibid.* **73**, 205 (1994); G. L. Gulley and R. Tao, Phys. Rev. E **56**, 4328 (1997); T. C. Halsey and W. Toor, J. Stat. Phys. **61**, 1257 (1990); T. C. Halsey and W. Toor, Phys. Rev. Lett. **65**, 2820 (1990); K. C. Hass, Phys. Rev. E **47**, 3362 (1993).
[13] S. Wolfram, *Mathematica™: A System for Doing Mathematics by Computer* (Addison-Wesley, Redwood City, CA, 1988).
[14] M. Parthasarathy and D. J. Klingenberg, Mater. Sci. Eng., R. **17**, 57 (1996).
[15] K. D. Weiss, J. D. Carlson, and J. P. Coulter, J. Intell. Mater. Syst. Struct. **4**, 13 (1993).
[16] C. F. Zukoski, Annu. Rev. Mater. Sci. **23**, 45 (1993).
[17] T. C. Jordan and M. T. Shaw, IEEE Trans. Electr. Insul. **24**, 849 (1989).
[18] H. Block, J. P. Kelly, A. Qin, and T. Watson, Langmuir **6**, 6 (1990).
[19] H. Block and J. P. Kelly, J. Phys. D **21**, 1661 (1988).
[20] Y. Chen and H. Conrad, in *Developments in Non-Newtonian Flows*, ASME Applied Mechanics Division, edited by D. A. Siginer, W. E. Van Arsdale, M. C. Altan, and A. N. Alexandrou (ASME, New York, 1993), Vol. 175, p. 199.
[21] X.-D. Pan and G. H. McKinley, J. Colloid Interface Sci. **195**, 101 (1997).
[22] X.-L. Tang, K.-Q. Zhu, E. Guan, and X.-P. Wu, in *Electrorheological Fluids: Mechanisms, Properties, Technology, and Applications*, edited by R. Tao and G. D. Roy (World Scientific, Singapore, 1994), p. 223.
[23] W. Wen and K. Lu, Phys. Fluids **9**, 1826 (1997).
[24] W. Wen and K. Lu, Phys. Fluids **8**, 2789 (1996).
[25] W. Wen and K. Lu, Phys. Rev. E **55**, R2100 (1997).
[26] W. Wen, D. W. Zheng, and K. N. Tu, Phys. Rev. E **58**, 7682 (1998).
[27] Electrical properties of constituent materials were taken from *CRC Handbook of Chemistry and Physics*, 72nd ed. (CRC Press, Boca Raton, FL, 1992); Dielectric Constant Reference Guide (ASI Instruments Inc., Houston, TX) (http://www.asiinstr.com); Dielectric Constants of Various Material (http://library.advanced.org/10784/dielectric_constants.html).
[28] S. Fraden, A. J. Hurd, and R. B. Meyer, Phys. Rev. Lett. **63**, 2373 (1989).
[29] Q.-H. Wei, X.-H. Liu, C.-H. Zhou, and N.-B. Ming, Phys. Rev. E **48**, 2786 (1993).
[30] H. P. Schwan, G. Schwarz, J. Maczuk, and H. Pauly, J. Phys. Chem. **66**, 2627 (1962).
[31] J. E. Martin, J. Odinek, and T. C. Halsey, Phys. Rev. Lett. **69**, 1524 (1992).
[32] J. E. Martin, J. Odinek, T. C. Halsey, and R. Kamien, Phys. Rev. E **57**, 756 (1998).
[33] K. L. Smith and G. G. Fuller, J. Colloid Interface Sci. **155**, 183 (1993).
[34] A. A. Teixeira-Pinto, L. L. Nejelski, J. L. Cutler, and J. H. Heller, Exp. Cell Res. **20**, 548 (1960).
[35] A. A. Furedi and R. C. Valentine, Biochim. Biophys. Acta **56**, 33 (1962).
[36] H. P. Schwan, Br. J. Cancer **45**, Suppl V, 220 (1982).
[37] H. P. Schwan, IEEE Trans. Dielectr. Electr. Insul. **EI-24**, 913 (1985).
[38] U. Zimmermann, in *Electromanipulation of Cells*, edited by U. Zimmermann and G. A. Neil (CRC Press, London, 1996), p. 173; Biochim. Biophys. Acta **694**, 227 (1982).
[39] W. Wen, H. Ma, W. Y. Tam, and P. Sheng, Phys. Rev. E **55**, 1294 (1997).
[40] A. Inoue, in *Proceedings of the Second International Conference on Electrorheological Fluids*, edited by J. D. Carlson, A. F. Sprecher, and H. Conrad (Technomic, Lancaster, PA, 1990), p. 176.
[41] J. M. Ginder and S. L. Ceccio, J. Rheol. **39**, 211 (1995).
[42] P. J. Rankin and D. J. Klingenberg, J. Rheol. **42**, 639 (1998).
[43] D. L. Klass and T. W. Martinek, J. Appl. Phys. **38**, 67 (1967).
[44] P. G. de Gennes and P. Pincus, Phys. Kondens. Mater. **11**, 189 (1970).
[45] K. Lu, W. Wen, C. Li, and S. Xie, Phys. Rev. E **52**, 6329 (1995).
[46] F. Kun and K. F. Pal, Phys. Rev. E **57**, 3216 (1998).